Photo induced absorption study of model organic charge transfer systems
by Amy Alta Elizabeth Hyfield

A thesis submitted in partial fulfillment of the requirements for the degree of Master of Science in Chemistry
Montana State University
© Copyright by Amy Alta Elizabeth Hyfield (2000)

Abstract:
The wide use of lasers and their potential as a harmful device has created a need for ways to intelligently block these intense light sources called optical limiters. Reverse Saturable Absorption (RSA) has been targeted as a type of non-linear process that can result' in optical limiting. This research focuses on achieving RSA through the formation of transient charged species such as polarons and bipolarons via photo induced charge transfer. In order to effectively engineer materials for this application, it is important to gain an understanding about the structure-property relationships that exist among the molecular systems as well as the processes occurring after photoexcitation. This thesis examines the general trends of the rate constants for diffusion limited forward and reverse electron transfer of novel organic donor molecules in solution with C60, a known electron acceptor. It also looks at the quantum efficiency of the formation of solvated ions calculated via their maximum absorbance and through a new method of determination involving an isobestic point. The quantum yield efficiency of C60 triplet quenching is also calculated and an attempt to reconcile the difference between this yield and the yield of solvated ions is presented.

/

PHOTO INDUCED ABSORPTION STUDY OF MODEL ORGANIC CHARGE TRANSFER SYSTEMS

by

Amy Alta Elizabeth Hyfield

A thesis submitted in partial fulfillment
of the requirements for the degree

of

Master of Science

in

Chemistry

MONTANA STATE UNIVERSITY
Bozeman, Montana

July 2000

N378
H9962

APPROVAL

of a thesis submitted by

Amy Hyfield

This thesis has been read by each member of the thesis committee and has been found to be satisfactory regarding content, English usage, format, citations, bibliographic style, and consistency, and is ready for submission to the College of Graduate Studies.

Dr. Lee Spangler — (Signature) — 7-20-2000 (Date)

Approved for the Department of Chemistry

Dr. Paul Grieco — (Signature) — 7-20-00 (Date)

Approved for the College of Graduate Studies

Dr. Bruce McLeod — (Signature) — 7-21-00 (Date)

STATEMENT OF PERMISSION TO USE

In presenting this thesis in partial fulfillment of the requirements for a master's degree at Montana State University, I agree that the Library shall make it available to borrowers under the rules of the Library.

If I have indicated my intentions to copyright this thesis by including a copyright notice page, copying is allowable only for scholarly purposes, consistent with "fair use" as prescribed in the U.S. Copyright Law. Requests for permission for extended quotation from or reproduction of this thesis in whole or in parts may be granted only by the copyright holder.

Signature 

Date 07·19·00

ACKNOWLEDGMENTS

I would like to thank Dr. Lee Spangler for his mentorship through my years at Montana State University. His knowledge, creativity and understanding are unparalleled. I would also like to thank the countless souls in the Department of Chemistry, the Department of Physics and throughout the University for their guidance and friendship. This includes, most especially: Dr. Charles Spangler and the C. Spangler group; the people of Scientific Materials Corporation; Dr. Pat Callis; Dr. David Singel; Mary McLaughlin and my lab mates, especially Wendi Sonnenberg, Yanong Han, Jeff Wilcox, Tony Smith, Hu Li and Tami Faircloth. As life requires balance, I must also thank my dear cycling buddies, who helped me maintain my sanity and perspective and my family, especially Milo, who have always supported me and my wild dreams.

I would also like to express my gratitude to the Montana Space Grant Consortium, which funded a large portion of this research though a Graduate Fellowship for the academic year 1999-2000. Additional funding for this project comes from the AFOSR, BMDO, ARO and Scientific Materials Corporation, Bozeman, MT.

TABLE OF CONTENTS

LIST OF TABLES vii

LIST OF FIGURES viii

LIST OF SCHEMES xi

ACRONYMS xii

ABSTRACT xiii

1. INTRODUCTION 1

Optical Limiting 1
Optical Limiting Mechanisms 2
Photo Induced Charge Transfer 3
Classical Charge Transfer Theory 5
Diffusion Limited Reactions 12
Statement of Problem 15
History 15
Current Molecules 17

2. FOURIER TRANSFORM SPECTROSCOPY 21

General 21
Operating Modes 23
Measuring PIA with FT Interferometry 25
Difference Method 28
Modulated Method 28
Time Resolved Method 29

3. EXPERIMENTAL PROCEDURE 31

Sample Materials 31
Instrumental 32

TABLE OF CONTENTS – CONTINUED

4. RESULTS AND DISCUSSION..... 36

Basic Absorption Measurements..... 36
Absorption of Transient Species..... 45
Calculating Rate Constants and Quantum Efficiency..... 47
Reverse Electron Transfer..... 50
Forward Electron Transfer..... 61
Quantum Efficiency..... 64

5. CONCLUSION..... 78

REFERENCES..... 82

LIST OF TABLES

Table Page

1. Compounds and Concentrations Studied..... 31

2. Absorption of Tested Species at 532nm..... 44

3. Molar Extinction Coefficients of the Polarons of the Molecules Studied..... 54

4. Average Recombination Rate Constants, k_{ET}, for the Molecules Studied with C_{60}..... 57

5. Average Forward Electron Transfer Rate Constants for Molecules Studied with C_{60}..... 64

6. Average Quantum Efficiency for Molecules Studied Using Calculated Rate Constants..... 66

7. Average Concentrations and Quantum Yields Calculated using $[D^+]_{max}$ and $[A^*]_{max}$ Values..... 68

8. Example Rate Constants for the Mechanism in Scheme 3..... 76

LIST OF FIGURES

Page

Figure

1. Reverse Saturable Absorption..... 3
2. Electron and Hole Transfer..... 4
3. Diagrams Showing the Intersection of the Gibbs Energy Surfaces for the Reactant (R) State (D|A) and the Product (P) State ($D^+|A^-$)..... 7
4. Potential Energy Diagram for the Quantum Mechanical Model of Electron Transfer..... 11
5. Oligimers n=1, n=2, and n=3 of the Bis-diphenylamino diphenylpolyene Series..... 16
6. 3 arm and 4 arm n=1 Dendrimers..... 18
7. Hydroxy Substituted diphenylamino diphenylpolyene Series..... 20
8. Michelson Interferometer..... 22
9. Step Scan Fourier Transform Interferometry..... 24
10. Pictorial Description of Aliasing..... 26
11. Basic Geometry for FT-PIA Experiments..... 27
12. Absorption Spectra for Neutral and Bipolaron (Doped) Kn1 Chromophore..... 38
13. Absorption Spectra for Neutral and Bipolaron (Doped) Kn2 Chromophore..... 39
14. Absorption Spectra for Neutral and Bipolaron (Doped) Kn3 Chromophore..... 40

LIST OF FIGURES - CONTINUED

Figure Page

15. Absorption Spectra for Neutral and Bipolaron (Doped) 4 arm Dendrimer.....41

16. Kn1 Series with C_{60} Absorption Compared to Absorption of C_{60} Alone.....42

17. Kn2 Series with C_{60} Absorption Compared to Absorption of C_{60} Alone.....42

18. Kn3 Series with C_{60} Absorption Compared to Absorption of C_{60} Alone.....43

19. 4 arm Dendrimer with C_{60} Absorption Compared to Absorption of C_{60} Alone.....43

20. Chemically Induced Absorption Spectra of 4 arm Dendrimer.....44

21. Cross Section of Potential Energy Surface of the Ground State ot the Polaron with Two Minima Showing a New Well and Intervalence Transitions Created by an Avoided Crossing.....45

22. Photo Induced Triplet – Triplet Absorption of C_{60}.....46

23. Difference Spectrum of 4 arm Dendrimer/C_{60} Solution.....47

24. PIA of the Kn1, Kn2 and Kn3 Oligimers with C_{60}.....48

25. Example of Linear Fit to Reciprocal Optical Density Data.....53

26. Kn2 Dendrimer Decay Curve with Linear Fit for Comparison.....56

27. Kn3 Dendron Decay Curve with Linear Fit for Comparison.....56

LIST OF FIGURES – CONTINUED

Figure Page

28. Kn3 Dendrimer Decay Curve with Linear Fit for Comparison.....57

29. Calculated Recombination Rate Constants, k_{ET}, for Kn1 Series.....58

30. Calculated Recombination Rate Constants, k_{ET}, for Kn2 Series.....58

31. Calculated Recombination Rate Constants, k_{ET}, for Kn3 Series.....59

32. Example of Isobestic Point in Kn3 Molecules.....71

33. Quantum Yield Efficiencies Calculated Using Isobestic Point Method.....72

LIST OF SCHEMES

Scheme Page

1. Mechanism for Charge Transfer..... 5

2. Mechanism for Charge Transfer Seen in the Molecules Studied.....49

3. Modified Mechanism for the Cooperative Processes Present in the Molecular Combinations Studied..... 75

ACRONYMS

A	Acceptor
D	Donor
FTIR	Fourier Transform Infrared Spectroscopy
FTS	Fourier Transform Spectroscopy
FTVIS	Fourier Transform Visible Spectroscopy
HeNe	Helium Neon laser
IADC	Internal Analog to Digital Converter
Kn1	Hydroxy substituted Diphenylamino diphenylpolyene with one double bond
Kn2	Hydroxy substituted Diphenylamino diphenylpolyene with two double bonds
Kn3	Hydroxy substituted Diphenylamino diphenylpolyene with three double bonds
n=1	Bis-(diphenylamino) diphenylpolyene with one double bond
n=2	Bis-(diphenylamino) diphenylpolyene with two double bonds
n=3	Bis-(diphenylamino) diphenylpolyene with three double bonds
OD	Optical Density
ODCB	o-dichlorobenzene
PIA	Photo Induced Absorption
PI-CT	Photo Induced Charge Transfer
RSA	Reverse Saturable Absorption

ABSTRACT

The wide use of lasers and their potential as a harmful device has created a need for ways to intelligently block these intense light sources called optical limiters. Reverse Saturable Absorption (RSA) has been targeted as a type of non-linear process that can result in optical limiting. This research focuses on achieving RSA through the formation of transient charged species such as polarons and bipolarons via photo induced charge transfer. In order to effectively engineer materials for this application, it is important to gain an understanding about the structure-property relationships that exist among the molecular systems as well as the processes occurring after photoexcitation. This thesis examines the general trends of the rate constants for diffusion limited forward and reverse electron transfer of novel organic donor molecules in solution with C_{60}, a known electron acceptor. It also looks at the quantum efficiency of the formation of solvated ions calculated via their maximum absorbance and through a new method of determination involving an isobestic point. The quantum yield efficiency of C_{60} triplet quenching is also calculated and an attempt to reconcile the difference between this yield and the yield of solvated ions is presented.

CHAPTER 1

INTRODUCTION

Optical Limiting

The introduction of the laser has revolutionized optical science and everyday life as well. Along with its beneficial applications in areas like medicine and research, come its unfortunate dangers. Lasers can be a high powered and destructive tool with the capability to easily blind or destroy optically sensitive materials such as detectors or eyes. Therefore, important research is being performed with the goal of developing more intelligent ways to block high-powered light sources.

Filters are currently the primary method used to attenuate lasers. They have the undesirable effect, however, of completely stopping all of the light at the wavelengths over which they are designed to protect, regardless of the light's intensity. The result is that a person or detector can not see these colors at all which can be inconvenient and dangerous. With the development of lasers in wavelengths ranging from the UV to the IR, protecting a device against a strike from the myriad of possibly damaging sources through the use of filters would render the device useless. This is why the development of a "smart" filter that is active over a broad wavelength range, known as an optical limiter, is necessary. An ideal optical limiter must fulfill several demands. It must be a passive

device; that is, the light that it is designed to protect against should activate the limiting mechanism. It should be transmissive to low levels of light, such as room light, but opaque at higher intensity levels. It should limit over a wide wavelength range and it should work on time scales as short as hundreds of femtoseconds as well as protect against CW sources. It should not damage easily and should be able to block multiple pulses. All of these demands do not necessarily need to be the burden of one compound. Several different materials, both organic and inorganic, can be used in tandem to bring about the desired effect.

Optical Limiting Mechanism

Many different mechanisms have been proposed to bring about optical limiting. The focus in this research is on Reverse Saturable Absorption (RSA). In this mechanism (see Figure 1), weak ground state absorption populates the first excited state of a molecule. At low light levels, few molecules absorb and therefore there is minimal population in this state. This being the case, other absorption pathways play a negligible part in the attenuation and the over all absorption of the molecule is linear. When the population in this excited state becomes appreciable, as in the case with an incident laser beam, other processes begin to play a role. From this excited state, the molecule can yield several different transient species that can have subsequent absorption. When these additional absorption processes "turn on" the result is non-linear absorption where one molecule absorbs two or more photons before relaxing back to its ground state. If the

higher level absorptions by these transient species are resonant with the ground state absorption, then optical limiting is the result.

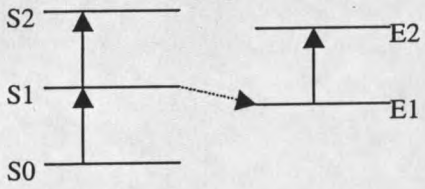

Figure 1. Reverse Saturable Absorption. S0 is the ground state, S1 is the first excited state, S2 is an additional excited state of the same molecule, E1 and E2 represent excited states of a different species

The nature of the transient depends on the compound being used. The transient can be either an excited singlet or triplet state. It could be an excited state of another molecule populated in energy transfer, or it could be an ionic state of either the photo-prepared molecule or another molecule generated by electron transfer. In any case, the transient species must be created quickly, efficiently and it should have a very strong absorption in order to optimize the RSA process.

Photo-induced Charge Transfer

The compounds under investigation in this study are known to form highly absorbing charged states when chemically oxidized. These cationic (polaron) and di-cationic (bipolaron) species are fairly stable and tunable over a wide range of wavelengths extending from ~ 500nm to ~1000nm depending on the conjugation length

in the molecule. These molecules could potentially be used for limiting if the absorption of the charged and neutral species sufficiently overlap and if the charged species can be photo-induced.

Photo-induced charge transfer has been seen in many different compounds, for instance, it is the initial step in photosynthesis. Two simple models have been proposed by Sariciftci and Heeger[1] to explain basic photo-induced charge transfer: electron transfer and hole transfer (see Figure 2). In electron transfer the donor molecule is prepared in an excited state by the absorption of a photon. The electron is then transferred to the LUMO of a nearby acceptor molecule. A cation and an anion result, each with new absorption capabilities. In hole transfer, the incoming light excites the acceptor. An electron from the HOMO of the donor molecule moves to the now vacant position in the HOMO of the acceptor, again yielding a cation and an anion.

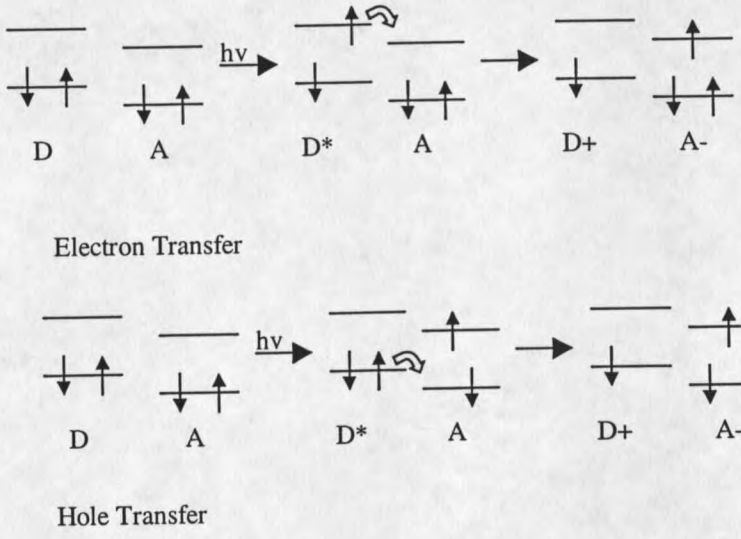

Figure 2. Electron and Hole Transfer. Charge can be transferred to create ions from neutral molecules through the transfer of an electron, top, or a hole, bottom. D is the donor molecule and A is the acceptor molecule.

Classical Charge Transfer Theory[2]

It is important to understand the process of electron transfer in order that the efficiency and rate with which ions are formed can be maximized. Much of the electron transfer theory today centers on the ideas of R.A. Marcus [2,3], who sought to describe outer-sphere electron transfer in ground state species, as well as additional work by Hush[2,4] and Rehm and Weller[5]. The ideas are easily applied to molecules in the excited state. The general mechanism for charge transfer goes as follows[2]:

$$D + A \underset{k_d}{\overset{k_a}{\rightleftharpoons}} D|A$$

$$D|A \underset{k_{-ET}}{\overset{k_{ET}}{\rightleftharpoons}} D^+|A^-$$

$$D^+|A^- \xrightarrow{k_{sol}} D^+ + A^-$$

Scheme 1. Mechanism for Charge Transfer. D is the donor molecule, A is the acceptor molecule, D | A represents a donor/acceptor complex

In the first step, the donor and acceptor molecule diffuse together to form a precursor complex D | A. This process is controlled by two rate constants, k_a and k_d, the rate of association and dissociation, respectively. k_a usually approaches the diffusion-controlled limit, on the order of 6×10^9 liters/mole-sec for neutral molecules in water[6]. In the second step, the precursor complex moves toward a transition state in which electron

transfer takes place to form a successor complex, $D^+ | A^-$. The movement toward a transition state involves solvent reorganization to account for the movement of the electron in the electron transfer step. In addition, due to the Franck-Condon principle, the nuclear configuration of the precursor and successor complexes at this transition state needs to be the same.

The kinetics of the electron transfer is a key parameter in the understanding of this process. The rate constants embody such elements as the potential energy of the different states, the reorganization energy, as well as the nature of the characters. The rate of electron transfer can be written as:

$$k_{ET} = \kappa_{el} \upsilon_n \exp\left[-\frac{(\lambda + \Delta G^0)^2}{4\lambda k_B T}\right] \qquad 1$$

Where k_{ET} is the rate constant of electron transfer, κ_{el} is the electronic transmission coefficient, usually taken to be 1, υ_n is the nuclear motion through the transition state ($\upsilon_n \sim 10^{13}$ s^{-1}), ΔG^0 is the Gibbs free energy, k_B is the Boltzman constant, T is the temperature and λ is the reorganization energy. Two of the most important parameters in this equation are the reorganization energy and the Gibbs free energy and so a brief examination of their components is useful.

ΔG^0 between the reactant state, D + A, and the product state, $D^+ + A^-$, is given by the following expression:

$$\Delta G^0 = e\left(E^0_{D+/D} - E^0_{A/A-}\right) + \omega^P - \omega^R \qquad 2$$

where e is the charge of an electron, $E^0_{D+/D}$ and $E^0_{A/A-}$ are the standard reduction potentials for D^+ and A^- and ω^P and ω^R correct for the work done when bringing D^+ and

A^- and D and A together, respectively and are usually negative. It is thus clear that the Gibbs free energy is smaller when the reduction potentials of the ionic species generated are similar. The electron transfer reaction can be visualized as intersecting Gibbs free energy curves when plotted along the reaction coordinate. These are approximated by parabolas and, according to Marcus theory, the curvature of the reactant and product curves are assumed to be the same. Figure 3 shows these curves under varying conditions.

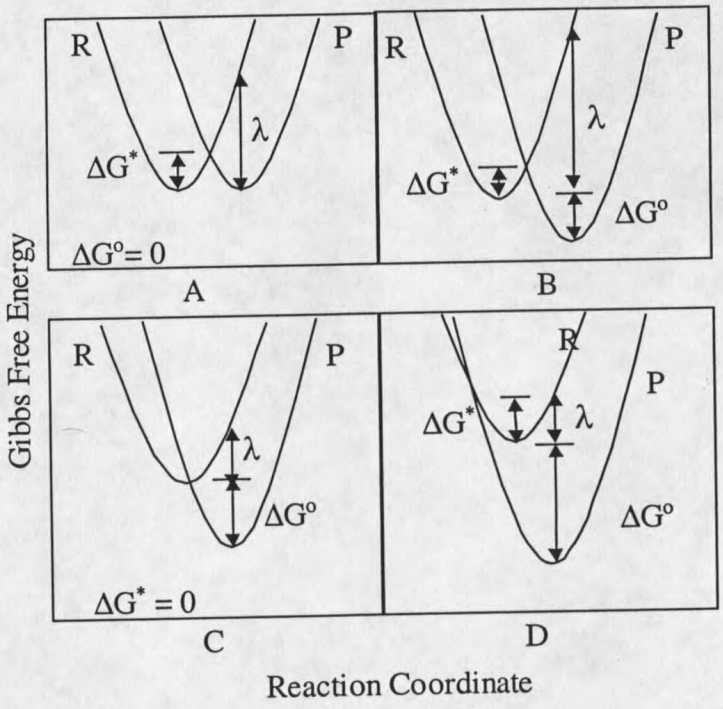

Figure 3. Diagrams Showing the Intersection of the Gibbs Energy Surfaces for the Reactant (R) State ($D \mid A$) and the Product (P) State ($D^+ \mid A^-$). (a) an isoergonic reaction with $\Delta G^0=0$; (b) the normal region where $0 \leq -\Delta G^0 \geq \lambda$ (c) the condition for maximum rate constant where $-\Delta G^0=\lambda$; (d) the "inverted region" where $-\Delta G^0 > \lambda$.[2]

Here we see the reorganization energy is defined as the change in the Gibbs free energy if the reactant state were to distort to the product state without the transfer of an electron. ΔG^* is the Gibbs energy of activation for the electron transfer reaction and ΔG^0 is the difference between the Gibbs energy of the reactant and product states when the donor and acceptor are a distance r_{DA} apart. ΔG^* is defined as

$$\Delta G^* = \frac{(\lambda + \Delta G^0)^2}{4\lambda} \qquad 3$$

Clearly, based on equations 1 and 3 and figure 3, the rate of electron transfer will increase and the activation energy will decrease as ΔG^0 becomes more negative, until the maximum rate is obtained at $-\Delta G^0 = \lambda$. If ΔG^0 becomes increasingly more negative, the rate is predicted to decrease again. This is known as the Marcus "inverted region".

The second important parameter in the rate equation is the reorganization energy, λ. This is usually made up of two contributing factors: the solvent- independent term, λ_{in} and the solvent-dependant term, λ_{out} , so that,

$$\lambda = \lambda_{in} + \lambda_{out} \qquad 4$$

λ_{in} is due to structural differences in the reactant and product equilibrium states. This is usually treated harmonically,

$$\lambda_{in} = \frac{1}{2}\sum_i \bar{f}_i \left(r_R^{eq} - r_P^{eq}\right)^2 \qquad 5$$

where r_R^{eq} and r_P^{eq} are the equilibrium bond lengths in the reactant and product states, respectively, $\bar{f}_i$ is the reduced force constant for the ith vibration and the sum is taken over all relevant intramolecular vibrations. λ_{out} is called the solvent reorganization energy

as it is due to the changes in orientation and polarization of the solvent induced by the transition from D | A to D^+ | A^-. In order to calculate this value, the solvent is treated as a dielectric continuum,

$$\lambda_{out} = \frac{1}{2}\varepsilon_0\left[\frac{1}{\varepsilon_{op}} - \frac{1}{\varepsilon_s}\right]\int\left(E^R - E^P\right)^2 dV \qquad 6$$

E^R and E^P are the electric field exerted in vacuum at a distance r from the centers of the reactant and product states, ε_{op} and ε_s are the optical and static dielectric constants of the solvent ($\varepsilon_{op} = n^2$ where n is the refractive index of the medium), and ε_0 is the permittivity of vacuum. A spherical reagent model is assumed so that the appropriate boundary conditions may be set for the integration, which is carried out over the volume. Ellipsoidal models have also been considered, but this generates more complex equations for λ_{out}. Therefore the equation after the integration is,

$$\lambda_{out} = \frac{(\Delta e)^2}{4\pi\varepsilon_0}\left[\frac{1}{2a_D} + \frac{1}{2a_A} - \frac{1}{r_{DA}}\right]\left[\frac{1}{\varepsilon_{op}} - \frac{1}{\varepsilon_s}\right] \qquad 7$$

Where Δe is the charge transferred, a_D and a_A are the atomic radii of the donor and acceptor and r_{DA} is the center to center distance between the donor and acceptor. In very non-polar solvents, $\varepsilon_{op} \approx \varepsilon_s$ and λ_{out} is very nearly zero. For very polar solvents, the solvent reorganization energy can be as much as 1.0-1.5 eV and becomes the dominating term in the total reorganization energy, λ. As stated before, the rate, k_{ET} reaches its maximum value when $-\Delta G^0 = \lambda$. Therefore, we can assume that a smaller λ means that the maximum rate can be achieved without having to have a more exergonic reaction.

However, non-polar solvents have other less desirable qualities, especially when one considers the entire electron transfer mechanism's efficiency, including back electron transfer and solvation of ions.

One of the assumptions made in this analysis is that κ_{el}, the electronic transmission coefficient, is equal to unity. This assumption implies that the reaction is adiabatic and there is a unit probability of electron transfer at the transition state. The electronic coupling energy, H_{rp}, is moderately large in this case and there is significant overlap between the equilibrium wave functions of the reactant and product states. Adiabatic charge transfer occurs when the donor and acceptor molecules are in close proximity (van der Waals contact or close intramolecular proximity) because H_{rp} falls off exponentially with distance. However, electron transfer can occur in cases where there is little electronic coupling, H_{rp} is small and $\kappa_{el} << 1$. This is non-adiabatic electron transfer and it can occur through three pathways. The first occurs when the nuclear configuration of the reactant and the product states are equivalent at the transition state and H_{rp} is small. The electron is transferred through electronic tunneling at the transition state (see Figure 4). The overall reaction rate is temperature dependant because of the extra energy needed to reach the intersection point. Secondly, the system can undergo activated nuclear tunneling. This occurs where the R and P surfaces are close enough for a thermally activated electron to tunnel from the reactant to the product state. It occurs at an activation energy below that of the intersection point (see wave function b of Figure 4) however, this method is still temperature dependent. The third type of non-adiabatic charge transfer is temperature-independent nuclear tunneling. This tunneling occurs from

the ground state of the reactant to the product state. It is not usually a very favorable transfer process and is illustrated by wave function c of Figure 4.

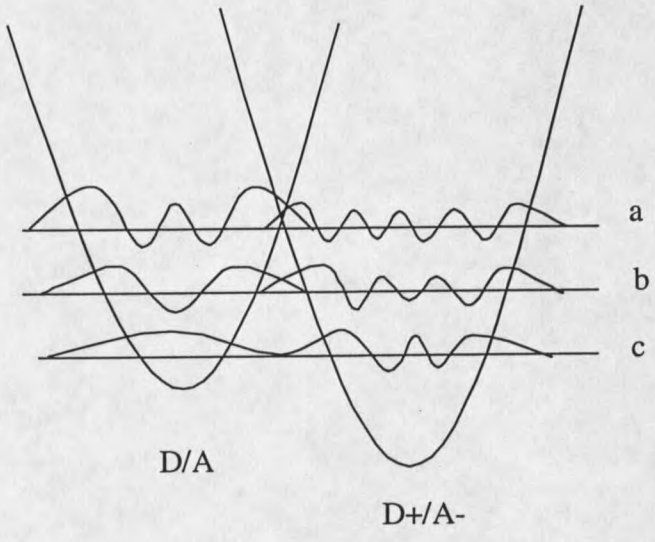

Figure 4. Potential Energy Diagram for the Quantum Mechanical Model of Electron Transfer. The vibrational wave functions are shown symbolically to illustrate tunneling. D/A and D+/A- indicate the reactant and product states respectively. Wave function a illustrates electron tunneling at the activation barrier, wave function b illustrates activated nuclear tunneling and wave function c shows temperature-independent nuclear tunneling.

The rate constant is dictated by Fermi's Golden Rule, that is, it is dictated by the square of the electronic interaction and the density of states. The quantum mechanical treatment of the electron transfer rate eventually coincides with the classical treatment (equation 1) as provided in the adiabatic case.

$$k_{ET} = \frac{2\pi}{\hbar} H_{rp}^2 (4\pi\lambda k_B T)^{\frac{-1}{2}} \exp\left[-\frac{(\lambda + \Delta G^0)^2}{4\lambda k_B T} \right] \qquad 8$$

Provided that

$$\kappa_{el}\nu_n = \frac{2\pi}{\hbar} H_{rp}^2 (4\pi\lambda k_B T)^{\frac{-1}{2}} \qquad 9$$

Clearly a compromise between solvent reorganization and Gibbs free energy exists that maximizes the electron transfer rate for the system. The difficulty is finding it for each particular system.

In many cases, especially in systems dealing with low concentrations in solution, the electron transfer rate is not the limiting rate, nor is it the only thing affecting the efficiency of the conversion. For instance, many electron transfer reactions in solution are diffusion limited.

Diffusion Limited Reactions[6]

The process of diffusion is fairly well understood and has been modeled for many different systems. The general phenomenological rate constant of a bimolecular reaction in solution is given by the following equation:

$$k = \frac{4\pi(D_A + D_B)\beta}{1 + [4\pi(D_A + D_B)\beta / k_R \exp\{-V(R)/k_B T\}]} \qquad 10$$

In this equation, D_A and D_B are the diffusion coefficients for molecules A and B respectively, β is calculated in the following way:

$$\beta^{-1} \equiv \int_R^\infty \frac{\exp(V(r)/k_B T)}{r^2} dr \qquad 11$$

V(r) is the potential energy, defined as:

$$V(r) = \frac{z_A z_B e^2}{\varepsilon r} \qquad 12$$

Where ε is the dielectric constant, z_A and z_B are the charges on molecules A and B respectively and e is the charge of an electron.

A diffusion limited reaction occurs when each encounter between the two molecules, A and B, results in a reaction. In this case, the rate constant for the reaction, k_R , is very large and the denominator for equation 10 becomes 1. If neutral molecules are considered, β = R and the diffusion limited rate constant becomes:

$$k_D = 4\pi(D_A + D_B)R \qquad 13$$

where R is the contact radius, $r_A + r_B$. The above equations were derived using a simple model that assumes spherical isotropic particles. The diffusion coefficient, D, is related to the viscosity of the solvent via the Einstein-Stokes relationship:

$$D = \frac{k_B T}{6\pi r \eta(T)} \qquad 14$$

Where η(T) is the temperature dependent viscosity of the solvent, r is the radius of the particle, k_B is the Boltzman constant and T is absolute temperature. The rate constant then becomes,

$$k_D = \frac{2k_B T(r_A + r_B)^2}{3\eta(T) r_A r_B} \qquad 15$$

In reactions involving ions, as in the recombination of the cationic and anionic species generated in photo-induced charge transfer, the potential energy term is no longer zero. β then becomes,

$$\beta = \frac{-z_A z_B r_0}{1-\exp(z_A z_B r_0 / R)} \qquad 16$$

where r_0 is given by the following equation:

$$r_0 = \frac{e^2}{\varepsilon k_B T} \qquad 17$$

Thus the diffusion limited rate constant for reactions involving ions is,

$$k_D = \frac{-4\pi(D_A + D_B)z_A z_B r_0}{1-\exp(z_A z_B r_0 / R)} \qquad 18$$

The diffusion limited rate constant of neutral species in solution compared to ions under similar conditions is dependent upon the ratio of β/R. For a system where $z_A z_B = -1$, as is the case here, this ratio is on the order of 2-10, depending on molecular size, with rate constants for solutions containing oppositely charged ions being larger than those for the neutral species. This is expected considering the coulombic attraction of oppositely charged particles.

Of course, when comparing rates of reaction, especially the forward electron transfer rate and the backward electron transfer rate (not geminate recombination) it is especially important to consider the concentration of the species involved. The concentration of the neutral species is, in many cases, significantly larger than that of the photo-induced ions.

Other solvent and solute specific parameters, such as charge state stability, orientation constraints, spin considerations and side reactions can affect the rates and the concentrations of species converted. Competing pathways such as radiative and non-radiative relaxation of excited species and back electron transfer diminish the overall

yield of the charged species that are to be used in optical limiting. Therefore, in order to understand and maximize the production of the charged species, the quantum efficiency of a photo-induced reaction can be determined. Measurement of the quantum efficiency of the reaction under various experimental conditions such as different solvents, concentrations and donor/ acceptor combinations gives information which will allow improvement in the efficiency of the charge transfer state formation and rational design of optical limiters.

Statement of Problem

History

The first class of compounds studied by the L.Spangler group as possible photo-induced absorbers and optical limiters was the bis-(diphenylamino) diphenylpolyene series depicted in Figure 5. The compounds posses many of the qualities that make them interesting for limiters study. Their ground state absorption in the visible is minimal, especially for the compounds with fewer double bonds, as they appear virtually colorless to orange. This allows for good visibility and color perception in a practical device. They are known to form chemically stable bipolaron states that have broad, intense absorptions. The possibility of polaron states exists as well, although they had not been chemically generated because it was thought that they would be unstable in solution. It remained to be seen, however, if the ionic states could be generated using light.

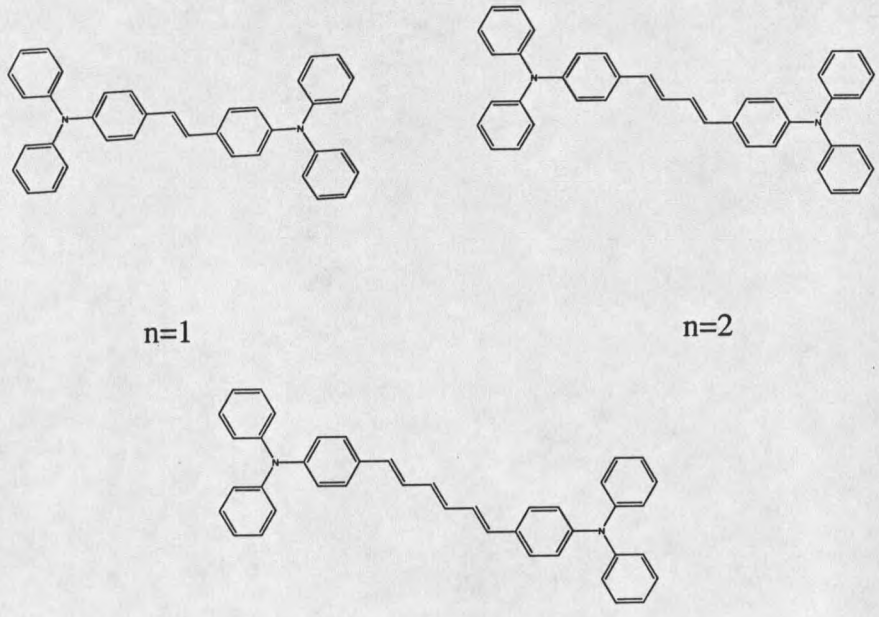

Figure 5. Oligimers n=1, n=2 and n=3 of the Bis-(diphenylamino) diphenylpolyene Series.

The molecule designated n=3 (due to the three double bonds in the polyene backbone) was the first to be tested. It was put in to o-dichlorobenzene with C_{60}, a known electron acceptor[7], in a 1:1 ratio. Upon excitation with 514nm and 488nm laser light from a CW Argon ion laser, three distinct PIA peaks were seen in the 15000 cm^{-1} to 10000 cm^{-1} region. The peaks were only present when the donor and acceptor were in solution together, indicating a cooperative effect. The identity of the peaks was at first uncertain; they did not display the broad, featureless absorption of the bipolaron and the λ_{max} was at the wrong wavelength for this species and the initial search for a corresponding anion or di-anion absorption was also fruitless.

An attempt to chemically generate the polaron of the bis-(diphenylamino) diphenylpolyene series was undertaken. A significantly diluted (1x 10^{-4}M) solution of antimony pentachloride was added dropwise to a solution containing the chromophore and spectra were taken after each addition of oxidizer. The resulting absorption spectrum was similar to that seen in the PIA spectra indicating the formation of a polaron in the photo induced experiment. Lower time resolved PIA spectra were taken of the donor-acceptor systems in the NIR region and the better signal to noise ratio afforded by these data allowed for positive identification of the C_{60}^- peak at 9300 cm^{-1} [8] confirming photoinduced charge transfer (PI-CT) in these systems.

The diphenylamine and polyene backbone moieties incorporated into these molecules were used in an attempt to enhance their non-linear capabilities. The extended pi-system promotes conjugation along the molecule's backbone which makes the molecule highly polarizable, an ideal trait for non-linear applications. In fact, the molecules are good two-photon absorbers. The conjugation permits delocalization and possibly stabilizes the cation and the dication formation. There is still some debate as to whether the charge remains localized on the nitrogen or if it is dispersed through the system. It was also speculated that a dendrimer based on these model chromophores would have enhanced capabilities due to the possibility of two dimensional conjugation.

Current Molecules

Two dendrimers based on the n=1 oligimer were synthesized (see Figure 6). which are designated the 3 arm and 4 arm n=1 dendrimers. Studies of the three arm dendrimer are discussed in Wendi Sonnenberg's thesis[9]. The PIA studies of the four arm

dendrimer including rates of solvated charged state formation and charge recombination, will be presented here.

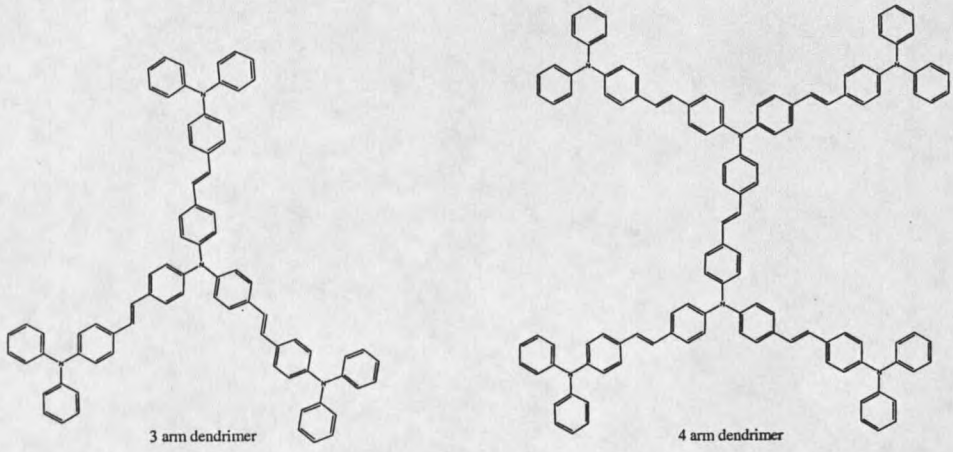

Figure 6. 3 arm and 4 arm n=1 Dendrimers.

The ultimate goal of this project is to create an optical limiting device. Ideally, such a material will be in a solid state form such as a polymer or gel or coated on to a solid substrate. Incorporation into a polymer backbone and easy dendrimer synthesis are desirable as one can control such parameters as the distance between donor and acceptor molecules as well as concentration of the chromophores. To this end, a new group of compounds with similar structural moieties to the original bis-(diphenylamino) diphenylpolyene series was synthesized by Kimba Ashworth in Dr. Charles Spangler's group[10]. These structures are pictured in Figure 7. They are very similar to the original series, however they have been modified with a hydroxy linkage to facilitate their addition into a polymer host as well as their formation into dendrons and dendrimers. The analysis of the PI-CT capabilities of this new group of materials will be investigated including a look at the solvated charge formation and charge recombination rates of these

compounds as well as a comparison between the charge transfer efficiency of the n=3 oligimer, dendron and dendrimer of this series as analyzed by the isobestic point method. A discussion of the original mechanism proposed and the modifications made necessary by quantum efficiency measurements is also a primary conclusion.

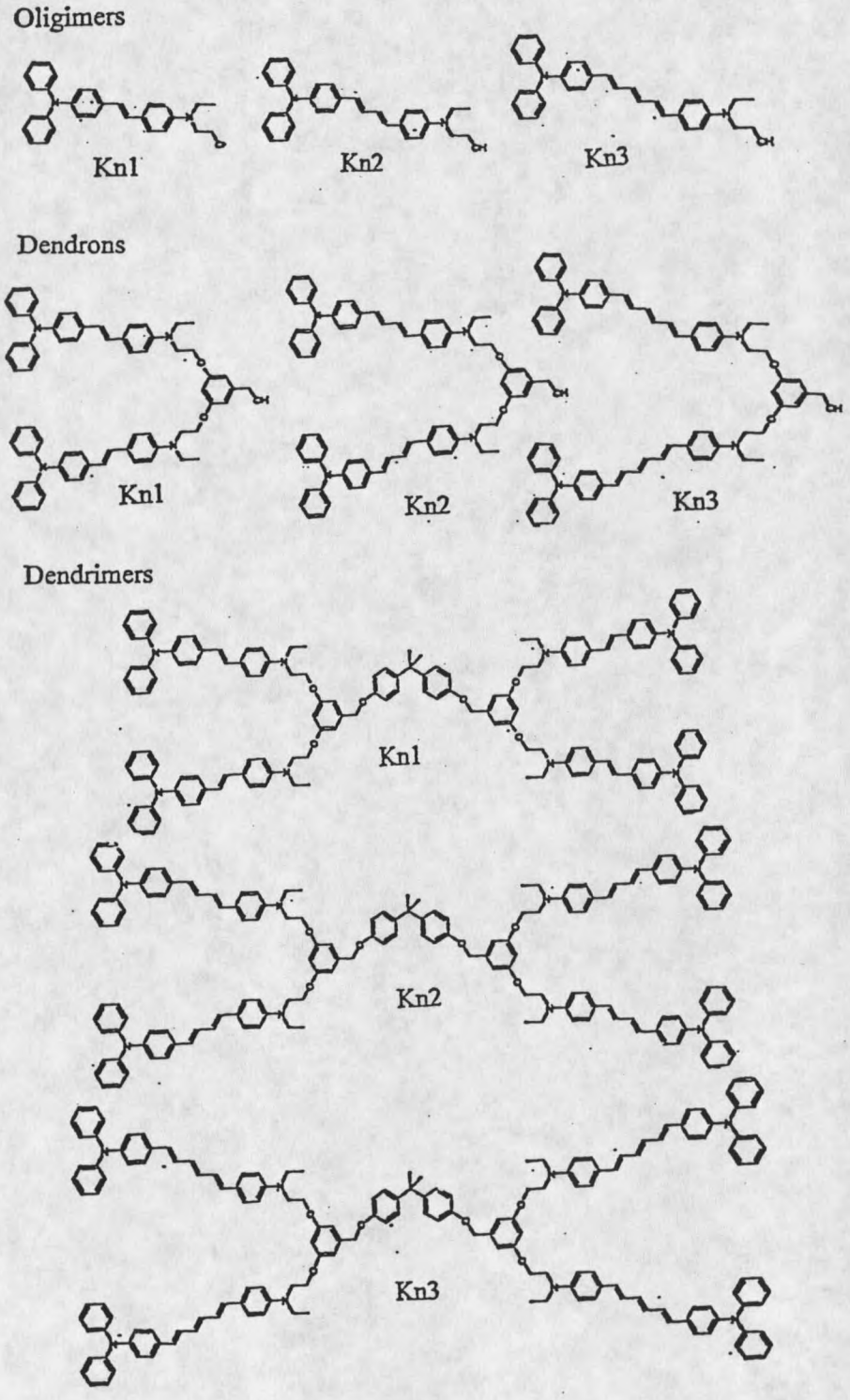

Figure 7. Hydroxy Substituted diphenylamino diphenylpolyenes Series. Kn1, Kn2 and Kn3 oligimers, dendrons and dendrimers

CHAPTER 2

FOURIER TRANSFORM SPECTROSCOPY

General

Fourier Transform Infrared (FTIR) and visible (FTVIS) spectroscopy have been used for many years as a trusted analytical tool. FTIR is especially prevalent in the identification of organic molecules through their characteristic absorptions in the "fingerprint region" of the mid-IR spectral region. Recently, Fourier Transform interferometry has become a very powerful tool in the analysis of time-resolved phenomena such as the dynamics of laser materials and, as will be shown here, transient absorption.

The FT instruments used in this study utilize a Michelson interferometer (Figure 8). The interferometer consists of two mirrors, one that is held stationary, M1, and one that can be moved, M2, and a beamsplitter, BS. Light enters the interferometer and is divided into two paths by the beamsplitter. Half of this light is reflected to the stationary mirror and half passes through to the moving mirror. The light is then reflected back along the same path by the respective mirrors and recombines at the beamsplitter where half of this light is transmitted and half is reflected. It is the transmitted light from the stationary mirror and the reflected light from the moving mirror that passes on to the detector. When the light from the two mirrors, M1 and M2, recombines at the

beamsplitter, it will interfere, providing a means of wavelength discrimination. The nature of the interference, that is constructive or destructive, depends on the relative pathlength difference that the light has traveled. The easiest way to picture this is to imagine a single frequency of light passing through the interferometer. If the stationary mirror is at a distance x from the beamsplitter, then the light will constructively interfere when the moving mirror is at a distance $(n * \lambda/2) + x$, ($n * \lambda$ total path length difference) from the beamsplitter, where n is an integer and λ is the wavelength of light. When the moving mirror is $(n * \lambda/4) + x$ ($n * \lambda/2$ total path length difference) from the beamsplitter, there is destructive interference. As the moving mirror is translated, the single frequency will oscillate between total constructive and total destructive interference. A plot of the intensity change versus mirror position (the mirror position can be converted to time using the path difference and the speed of light), known as an interferogram, yields a sine wave. The Fourier transform of this sine wave gives a delta function at the frequency of the light used.

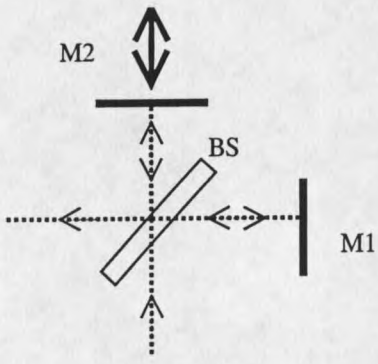

Figure 8. Michelson Interferometer. M1: Stationary mirror; M2: Moving mirror; BS: Beamsplitter; dashed line: light path.

If white light is passed through the interferometer, the different wavelengths of light will have differing levels of interference at each mirror position. Therefore, a more complex interfereogram is obtained. Nonetheless, a Fourier transform of this data will give the original frequencies and their intensities. It is the ability to differentiate between light frequencies while simultaneously transmitting these wavelengths, known as the multiplex advantage, that is an attractive feature of FT instruments.

Operating Modes

Typically, the interferometer is operated in continuous scan mode. In this case, the moving mirror is cycled through the necessary path length at a constant velocity. The position of the moving mirror is determined by using the interference pattern of a reference laser (in this case, a Helium Neon, HeNe, laser at 632.8 nm). Data is collected at every "zero crossing" or every time the sine wave value is zero. Continuous scan operation is generally used to take absorption or CW emission spectra.

The interferometer can also be used in step scan mode in order to take time resolved spectra (Figure 9). In this case, the interferometer is used in conjunction with a modulated or pulsed source, such as a pulsed laser. The moving mirror is stepped to a certain position and held there as the detector signal is digitized at multiple points in time using a transient digitizer. The temporal resolution can be set by the user and is currently limited by the response time of the detector and the speed of the electronics. The typical limit of resolution in the L. Spangler lab is 25-50ns. The mirror is then moved

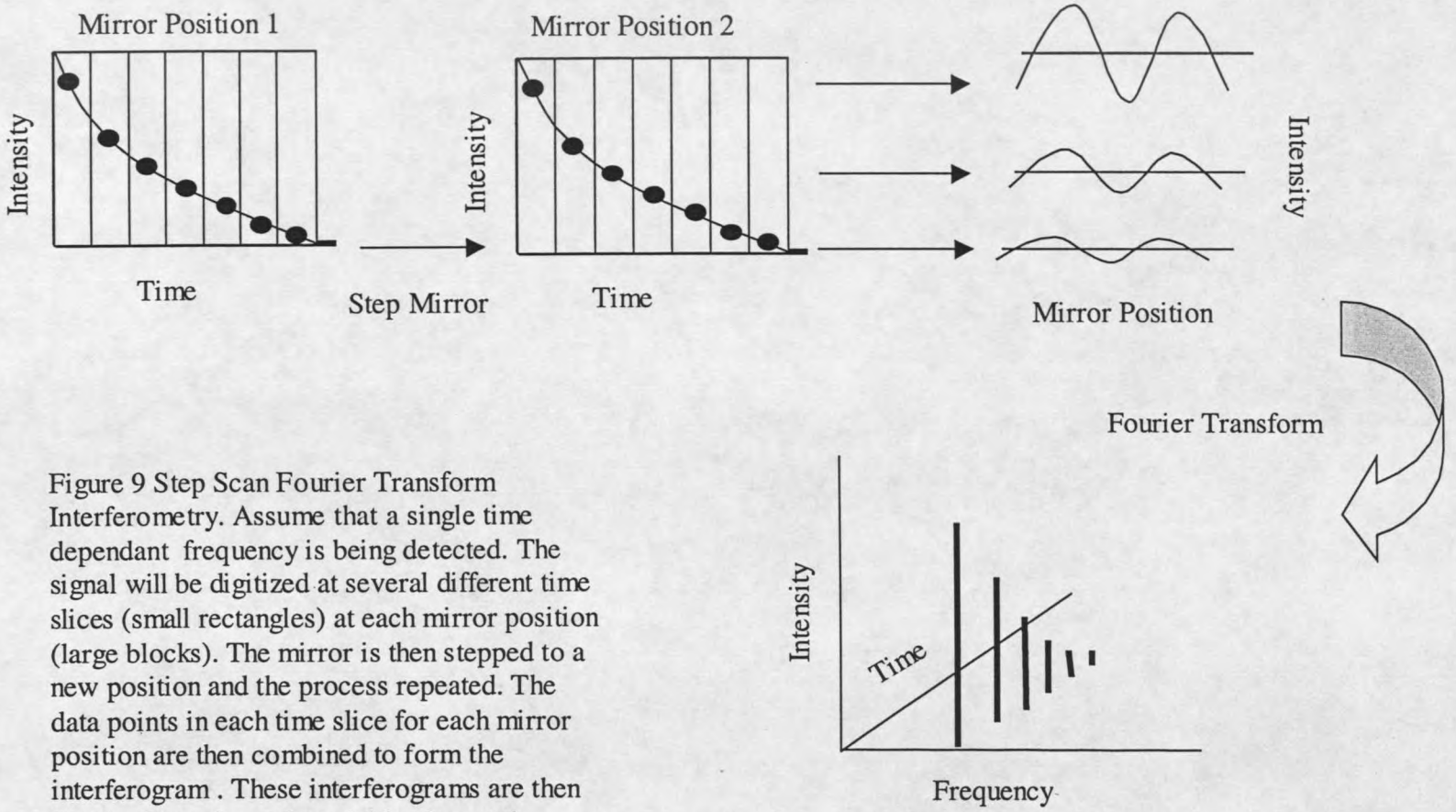

Figure 9 Step Scan Fourier Transform Interferometry. Assume that a single time dependant frequency is being detected. The signal will be digitized at several different time slices (small rectangles) at each mirror position (large blocks). The mirror is then stepped to a new position and the process repeated. The data points in each time slice for each mirror position are then combined to form the interferogram . These interferograms are then Fourier Transformed to yield a time and frequency resolved spectrum of the signal.

to a new position and time dependant data is collected again. In order to get better signal to noise, data acquisition at each mirror position can be repeated and the values averaged, referred to as co-additions. Step scan mode generates a three dimensional array of data consisting of time, mirror position and intensity. If the intensity reading at each mirror position for one time slice is compiled, a interfereogram at that time is generated. This can then be repeated for each time slice and these interferograms are then Fourier transformed to generate a time and frequency resolved spectra.

Measuring PIA with FT Interferometry

Fourier transform spectroscopy (FTS) was applied by the L. Spangler group to measure PIA spectra. Typically, PIA spectra are measured using dispersive instruments, the main disadvantage of which is the time required to gather complete time and frequency resolved data. In order to gather time resolved data with fine temporal resolution, a monochromator must sacrifice either wavelength resolution or spectral range, as it cannot scan a high spectral resolution spectrum across many wavelengths in a short period of time. Therefore, temporal traces are often gathered at one wavelength at a time. A large spectral region can therefore take a significant period to sample, especially at high resolution. In contrast, a relatively high resolution (100 cm^{-1}, 50ns) data set takes approximately 20 minutes or less with good signal to noise using step-scan FT methods.

A major disadvantage to using an interferometer for taking step-scan data is the current inability to collect spectral data on both sides of the HeNe reference laser at one time. This limitation is due to electronics involved in data acquisition. This means that

spectral information near the HeNe wavelength is difficult to obtain, due to the cut-off filters that must be used to prevent "folding". Folding or aliasing is a problem that plagues Fourier transform instruments if the spectral region that is to be treated is smaller than the region that the detector can detect. Figure 10 explains the process pictorially.

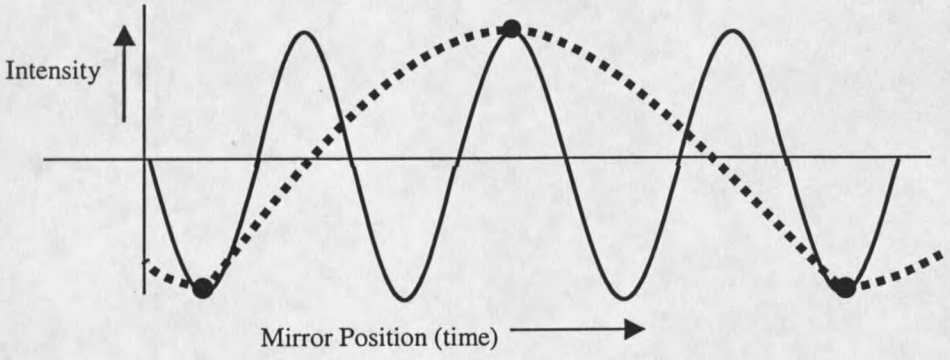

Figure 10. Pictorial Description of Aliasing. Points represent positions of data digitization. The solid line is actual frequency and the dashed line is aliased frequency .

The points that are digitized by the detector in Figure 10 are actually due to the frequency designated by the solid line. This frequency can be detected by the system, but is outside of the region to be Fourier transformed. The frequency designated by the dashed line also fits these points and is in the frequency range covered by the FT. This frequency will therefore appear in the resulting spectrum, even though it does not actually exist. In order to prevent this effect from entering into spectra, it is necessary to block all light outside of the Fourier transform region. The problem of not being able to cross the HeNe in step scan mode is currently being addressed by the L. Spangler group.

Three methods for characterizing PIA using FTS are being used. All involve the same experimental geometry illustrated in Figure 11. White light from a quartz tungsten halogen bulb passes through the sample and then into the interferometer. A laser beam is directed though the same sample volume in a quasi co-linear alignment. This laser is either CW, modulated or pulsed, depending on the experiment. The signal from the interferometer can be treated in a variety of ways as will be described.

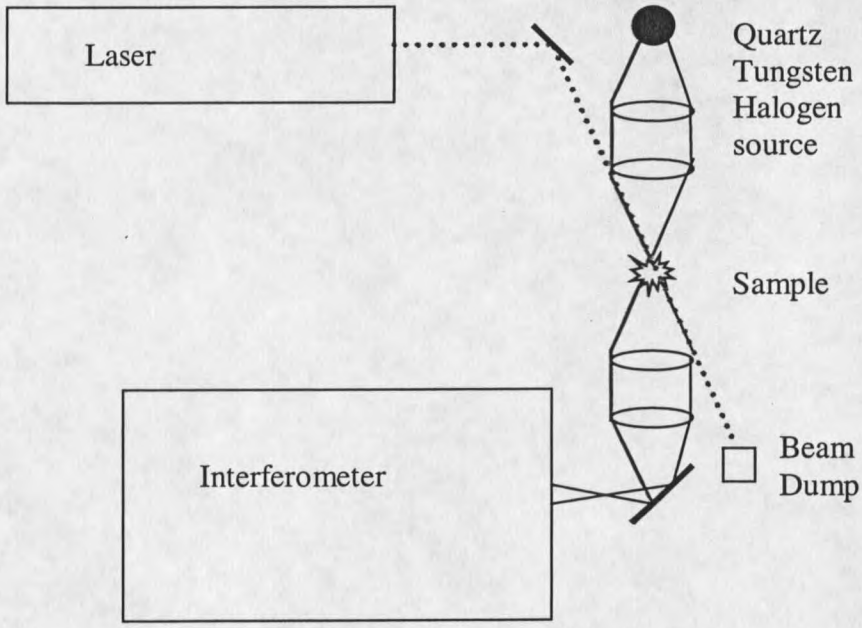

Figure 11. Basic Geometry for FT-PIA Experiments. The QTH bulb is the probe source and the laser is the pump source. The laser can be CW, mechanically modulated or pulsed.

Difference Method

The most simple PIA experiment involves taking sufficiently accurate absorption spectra of the sample with a CW (or effectively CW) laser incident upon the sample as well as with the laser off. The difference between these two spectra is divided by the ground state absorption, or unpumped, spectrum to generate the PIA curve. This data is not time resolved and merely gives wavelength and steady–state intensity information. The sensitivity of the measurement depends upon the signal to noise of the individual spectra taken.

Modulated Method

The second method involves a conceptually different way at obtaining difference spectra. Phase-sensitive detection is used in this case, which is usually more sensitive to small changes in intensity. The laser is modulated using a mechanical chopper. The detector signal from the interferometer is then fed into a lock-in amplifier, which is synchronized to the reference signal provided by the chopper and only amplifies signals that modulate at the same frequency as the laser pulse. There are two signals that occur at this frequency: laser induced emission and laser induced changes in the absorption of the white light. Emission and photo-induced transparency are easily distinguished from PIA based on their phase relationship to the laser pulse. The signal that comes out of the lock-in amplifier is therefore the difference between the absorption of the material with the laser on and with the laser off. This signal is fed back into the interferometer which is being operated in step scan mode. At each mirror position, a data point (or several if

averaging is desired) is taken after a user defined delay time which is adjusted to account for the time constant of the lock-in. The data points are then compiled into an interferogram and the resulting spectrum is divided by a spectrum of the sample's ground state absorption. Careful consideration must be placed on the differences in gain settings used to collect these two spectra if accurate intensity values are to be generated. This data is not time resolved and the acquisition tends to favor longer lived species as the lock-in amplifier effectively integrates the peaks in time. This method is good at providing the position of peaks with high sensitivity.

Time Resolved Method

The most informative method of data collection is time resolved PIA using the step scan FT instrument which has been described above. A pulsed laser is used as the pump source to create the transient species and the signal that is digitized is the white light probe which yields broadband absorption information. Several time traces are taken before the laser hits the sample, which provide ground state absorption information about the sample. All of the time resolved traces are subtracted from the average of the traces taken before the pump (unpumped traces) to give the absorption difference. In order to correct for the instrument and filter response, as is typically done, the difference spectra are then divided by the average unpumped trace to give $\Delta T/T$. The result is the temporal behavior of the absorption of the transient species created when the laser pulse encounters the sample. Because the spectra are fully time and frequency resolved, it is possible to watch the transfer of population from one species to another and to identify

possible intermediates that may not have been so easily spotted using other methods as well as extract valuable kinetic data and quantum efficiencies.

CHAPTER 3

EXPERIMENTAL PROCEDURE

Sample Materials

Purified donor samples were obtained from Dr. Charles Spangler's research group at Montana State University. All samples were powders and ranged in color from bright yellow to orange-red. C_{60} was obtained from Texas Fullerenes Corporation at 99% purity. Solutions were made using o-dichlorobenzene (ODCB), 99.9 % or CH_2Cl_2, HPLC grade from Fisher Chemical Company as solvent. The concentrations of each donor/acceptor solution tested are listed in Table 1.

Compound	Concentration	Compound	Concentration
KN1 oligimer/C_{60}	0.5mM/0.5mM	KN2 dendrimer/C_{60}	0.5mM/0.5mM
KN1 dendron/C_{60}	0.5mM/0.5mM	KN3 oligimer/C_{60}	0.5mM/0.5mM
KN1 dendrimer/C_{60}	0.5mM/0.5mM	KN3 dendron/C_{60}	0.5mM/0.5mM
KN2 oligimer/C_{60}	0.5mM/0.5mM	KN3 dendrimer/C_{60}	0.5mM/0.5mM
KN2 dendron/C_{60}	0.5mM/0.5mM	4arm dendrimer/C_{60}	0.1mM/0.1mM, 0.25mM/0.25 mM, 0.5mM/0.5mM, 1.0mM/0. 5mM

Table 1. Compounds and Concentrations Studied

Instrumental

Approximately 2mL of the solutions was placed in quartz or glass cuvettes with 1 cm path length obtained from Starna Cells Inc. The cells were cleaned using either a base or acid bath with a distilled water rinse. The outside of the cells was cleaned with either HPLC grade acetone or methanol. Nitrogen gas was bubbled through the samples for approximately twenty minutes before PIA testing to de-oxygenate and then sealed with Teflon caps and Parafilm.

Absorption spectra of the chromophore alone, bipolaron and the chromophore with C_{60} were taken on a Bruker IFS88 interferometer and a Shimadzu 3101PS UV/VIS instrument which had better performance in the UV and blue spectral regions. The solvent, CH_2Cl_2 for chromophore alone and bipolaron and ODCB for donor acceptor systems, was used for the background.

Spectra of chemically oxidized polarons were collected using the Bruker IFS 88. The quartz beamsplitter and silicon diode detector were used, as the region of interest extended from 25000 cm^{-1} to 10000 cm^{-1} . 2 mL of a solution of the chromophore at 1 x 10^{-5}M in CH_2Cl_2 was placed in an open cuvette which was gently stirred to encourage thorough mixing, yet not disturb the light passing through the sample. A solution of 2 x10^{-4} M $SbCl_5$ in CH_2Cl_2 was added dropwise to the cuvette via a 1 cc syringe and a fine gauge needle. A spectrum was taken after each addition of oxidizer (usually 5-10 drops at a time) until 2mL of the $SbCl_5$ had been added. These spectra were divided by the ground state absorption spectrum of the neutral chromophore.

Difference and modulated PIA measurements used the Bruker IFS 88 interferometer and a Coherent Sabre Argon ion laser to pump the samples at 488nm and 514nm. The beam was turned using right angle prisms and the full beam waist of approximately 5mm was used. The power of the beam was adjusted to 200-250mW by controlling the current supplied to the Ar^+ tube. In the case of the modulated experiments, a PTI OC4000 mechanical chopper was used with a modulation range of 1-1000 Hz. The white light probe was a quartz tungsten halogen bulb encased in a water cooled jacket. This housing was placed inside of a wooden box with a one inch diameter aperture in order to further stabilize the lamp temperature. The light was focused through the sample with a long focal length so that the diameter of the probe beam did not change too much through the cuvette. It was then collimated and re-focused with lenses appropriate for matching the interferometer's F/4.5 optical system. An adjustable iris was placed at the external focal point of the interferometer so that the light could be attenuated to prevent saturating the detectors and electronics. Filters to cut stray laser light were placed in the sample chamber. The Si/quartz detector/beam splitter combination was again used. A model SR510 lock-in amplifier from Stanford Research Systems was used for the modulated method with an AC-coupled detector. Spectra were taken with the laser off and with the laser on in the case of the difference method or with the laser on while being chopped in the case of the modulated method, which were then treated to yield the PIA of the sample.

Time resolved PIA spectra were taken using the Bruker IFS 66 interferometer. The pump source was the doubled output (532nm) of a Coherent Infinity 40-100

Nd:YAG laser operating at 50 Hz. The pulse is TEM_{00} and has a length of approximately ~7ns. In order to maintain stability of the laser and reduce pulse to pulse fluctuations to a standard deviation of ~1%, the laser was operated at a voltage sufficient to produce 250mJ of the fundamental (1064nm) or higher. The beam was directed using 532nm dichroic mirrors which passed the fundamental 1064nm beam that runs co-linearly with the 532nm, acting as a effective filter. The beam was split by a 70-30 beamsplitter and the beam of lower magnitude was then directed through a CaF_2 Glan-Laser polarizer and a filter to control the attenuation of the beam and therefore the power. The polarizer was adjusted so that the average energy of one pulse was 1.2 mJ. In order to control the diameter of the beam, a fixed aperture was placed in the path just before the laser encountered the sample. Filters, consisting most often of a red pass filter and an additional filter designed to block as much of the laser light as possible, were placed in the internal sample chamber of the interferometer. The silicon diode detector and quartz beam splitter were used for the 25000 cm^{-1} to 10000 cm^{-1} spectral region. A liquid nitrogen cooled InSb detector and a CaF_2 beam splitter were used for the 16,000 cm^{-1} to 2000 cm^{-1} region. Two temporal regimes were examined and each required the use of fast pre-amplifiers with the detectors. Data taken at 5 μsec time resolution used the internal analog to digital converter (IADC) while that taken at 50 nsec resolution required the PAD32 board, which has faster time response than the IADC.

All data was acquired using OPUS 3.1 which is the software that is included with the interferometers. Time resolved data was acquired with 200cm^{-1} spectral resolution and either 101 time slices at 5 μsec or 401 time slices at 50 nsec temporal resolution with

80 co-additions. Optical density calculations and optical density versus time traces were generated using OPUS and the exponential and linear fits to the data were performed using Microcal Origin version 4.10.

CHAPTER 4

RESULTS AND DISCUSSION

Basic Absorption Measurements

Initially, absorption spectra were taken of the various compounds tested (Figures 12-15)[10] as well as the compounds in solution with C_{60} (Figures 16-19). Each of the donor molecules has minimal absorption in the visible which is ideal for optical limiting applications. The acceptor, C_{60}, does have absorption in the visible region, however, it is possible to reduce this to a more desirable transmittance level by adjusting the concentration as long as efficiency is not compromised. The absorption at 532nm , given in Table 2, was of primary concern as this is where the molecules were to be excited. It was determined that C_{60} is the primary absorber at this wavelength for the Kn1, Kn2 and the 4 arm dendrimer solutions. Kn3 absorbs a small amount at 532nm, which was evidenced both by the absorption spectrum and by the presence of laser induced emission. Importantly, the ground state absorption of the donor and acceptor together in solution revealed no appreciable ground state charge complex formation; the absorption spectrum is just the combination of the two species' absorptions were they alone in solution.

The polaron of the 4 arm dendrimer was the only species in this study to be chemically induced. This was mainly due to the availability of the compound, as there

was a minimal amount of the hydroxy series with which to work. New solutions at 0.01mM were made because chemical oxidation required the use of methylene chloride as a solvent because $SbCl_5$ will oxidize the benzene ring in ODCB. The chemically oxidized absorption spectrum of the 4arm dendrimer exhibits peaks very similar to those seen in the chemically and photoinduced spectrum of the original bis-(diphenylamino) diphenylpolyene oligimer with one double bond (n=1) seen in Figure 5. This is expected as it is the parent molecule of the dendrimer. The visible peak is broad and fairly featureless (Figure 20), although on close examination it does display small bumps which bear resemblance to the two or three more distinct peaks of the polarons of the molecules in the same series with longer conjugation lengths. The detectable IR peaks in this series have a strong absorption cross section and are gaussian type bands. The peak in the IR region for the 4 arm dendrimer is significantly more red shifted than the IR peak of n=1 oligimer. This absorption may be due to a intervalence transition between the ground state potential well of the polaron and a potential well created by the avoided crossing of the different minima present in the molecule[11,12,13,14], presumably located at the nitrogens (Figure 21). It is clear that the dendrimer behaves in a qualitatively similar fashion to the n=1 oligimer in the visible region of the spectrum, where the development of optical limiters is currently focused.

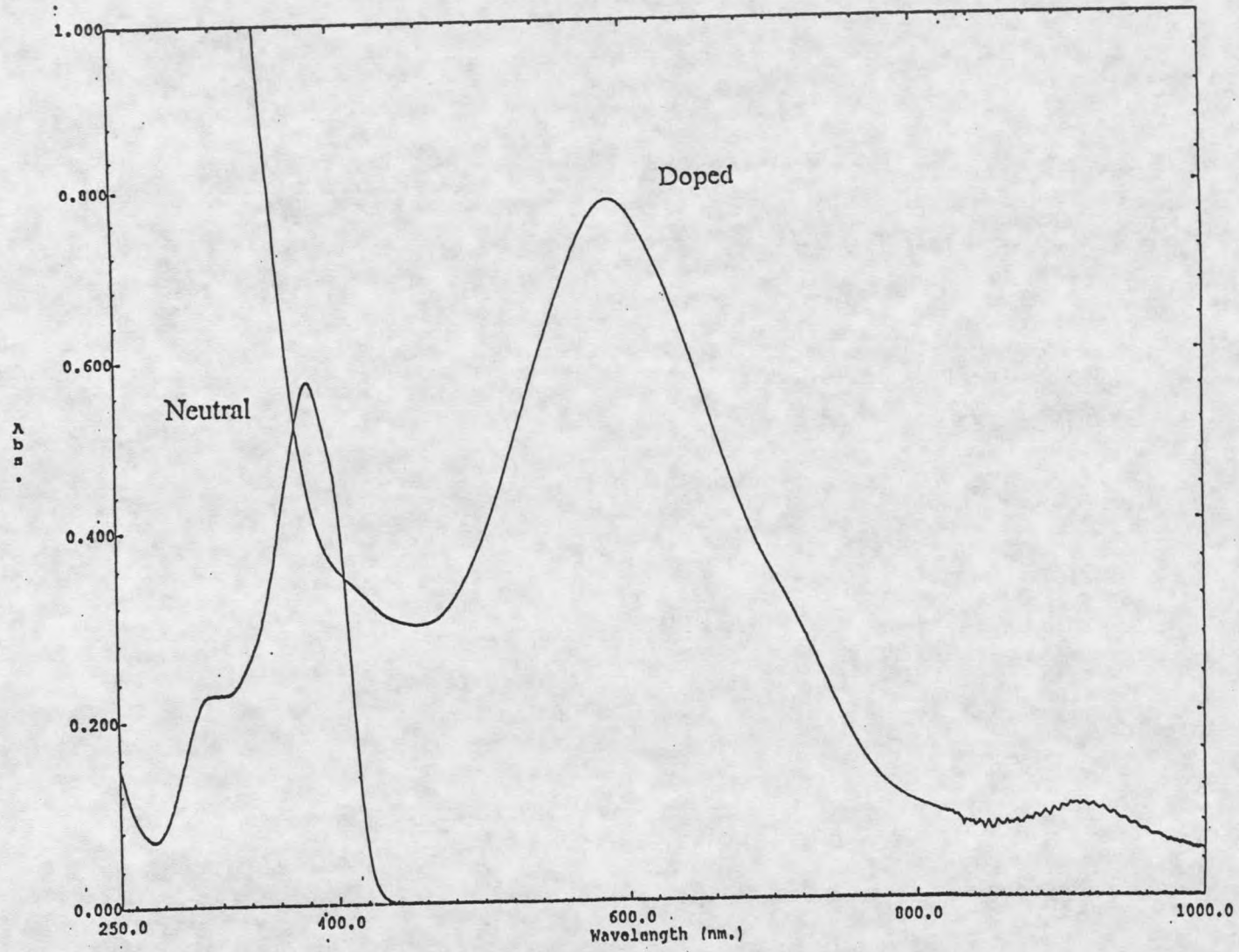

Figure 12. Absorption Spectra for Neutral and Bipolaron (Doped) Kn1 Chromophore

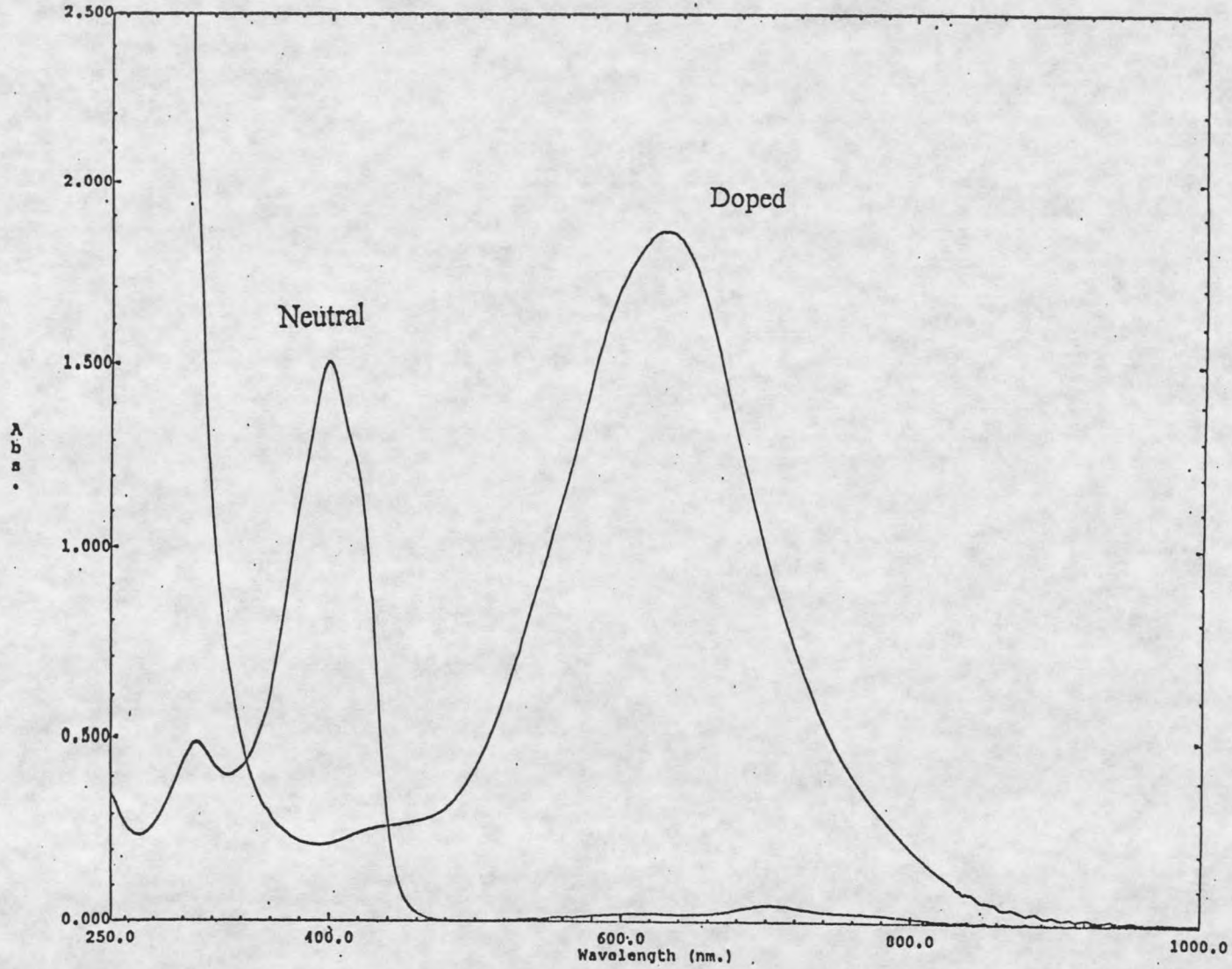

Figure 13. Absorption Spectra for Neutral and Bipolaron (Doped) Kn2 Chromophore

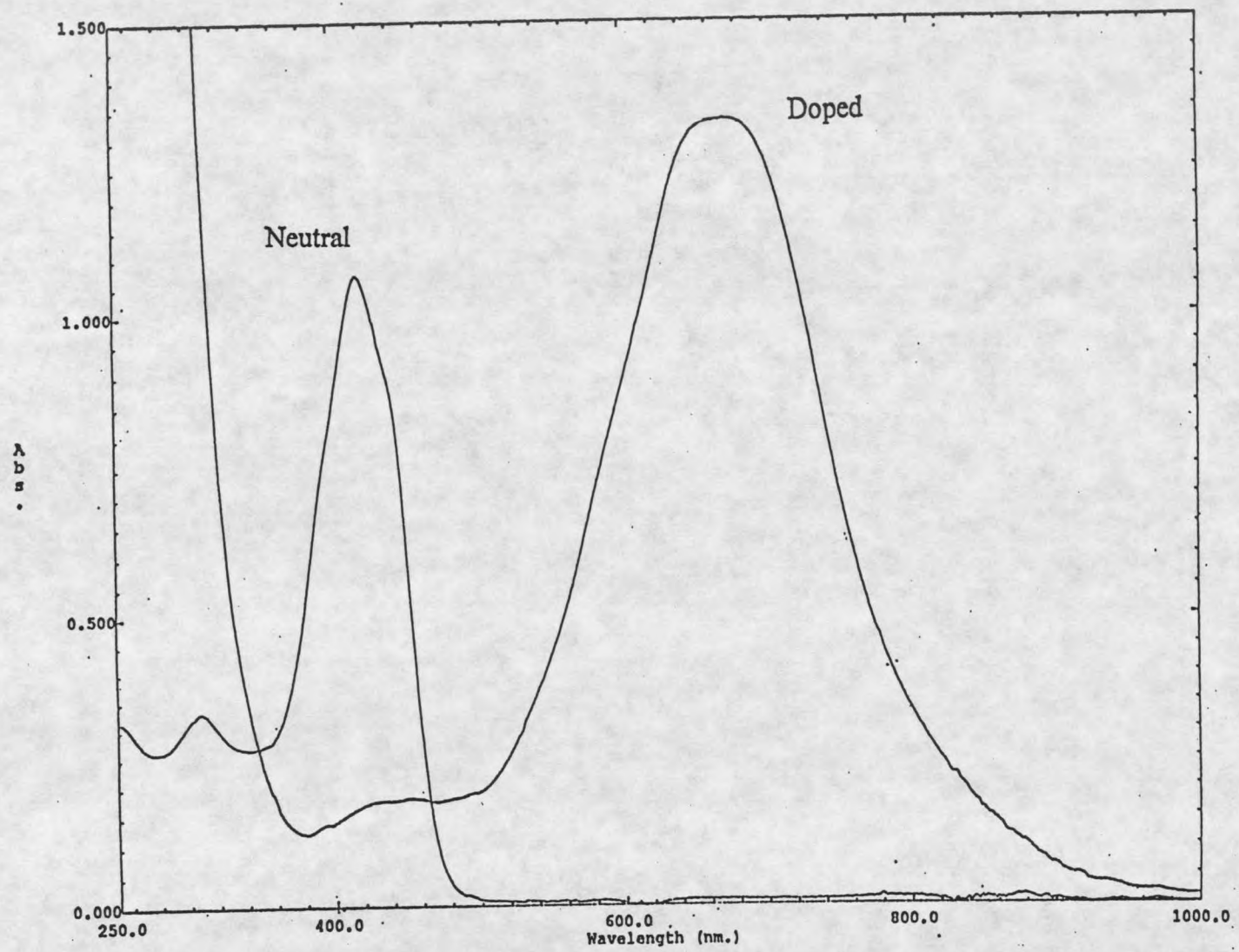

Figure 14. Absorption Spectra for Neutral and Bipolaron (Doped) Kn3 Chromophore

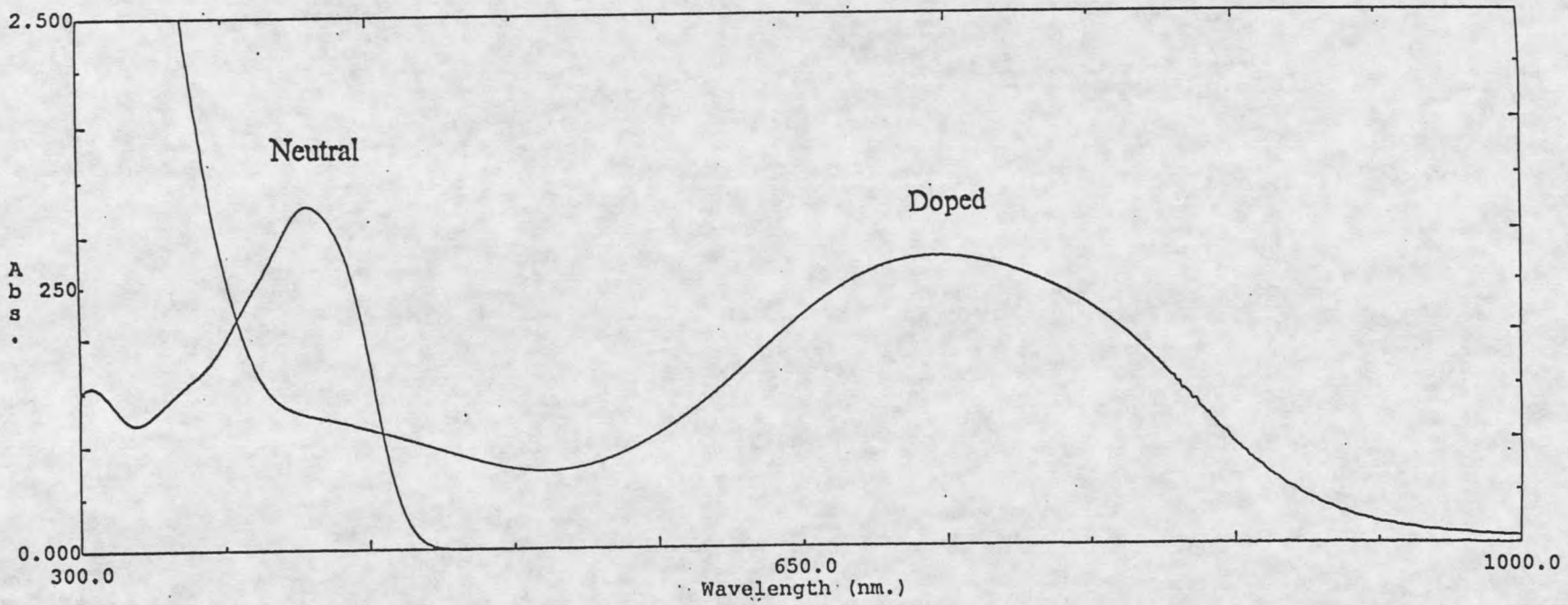

Figure 15. Absorption Spectra for Neutral and Bipolaron (Doped) 4 arm Dendrimer.

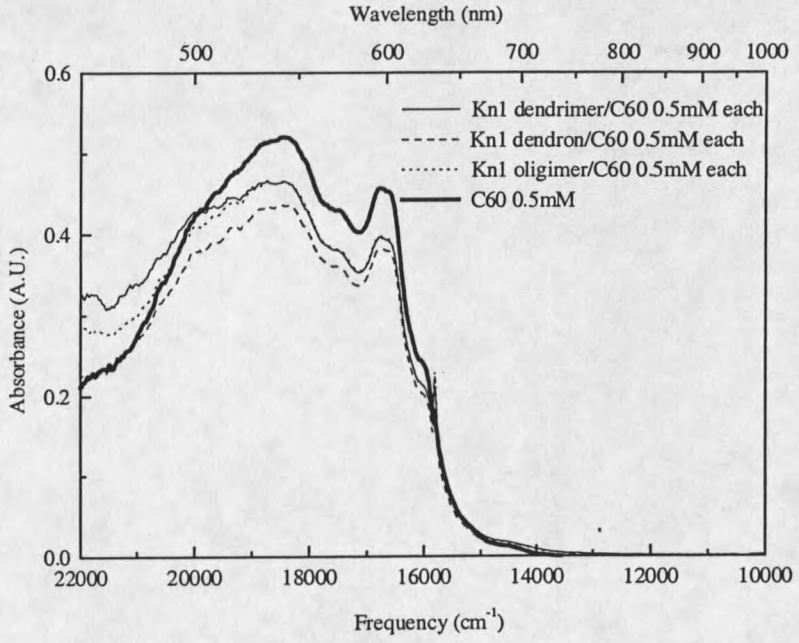

Figure 16. Kn1 series with C_{60} Absorption compared to Absorption of C_{60} Alone.

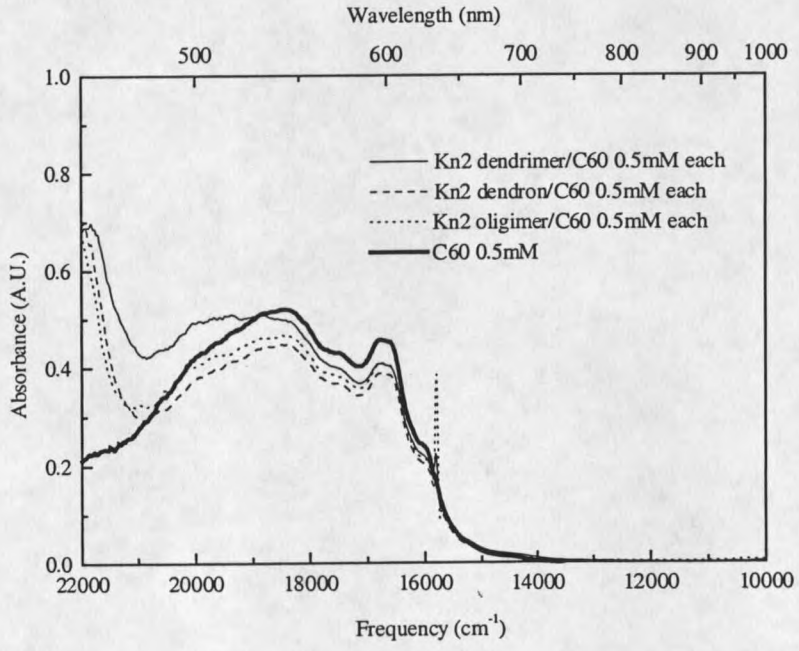

Figure 17. Kn2 Series with C_{60} Absorption Compared to Absorption of C_{60} Alone.

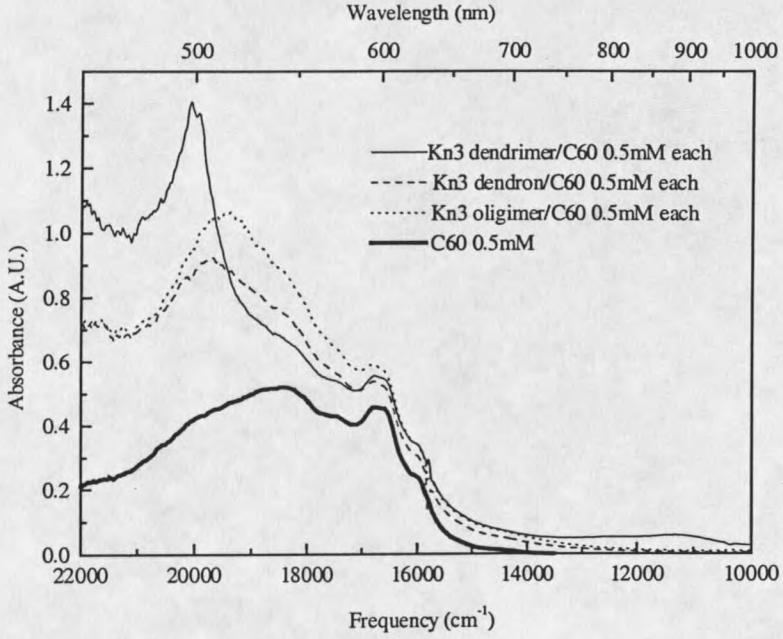

Figure 18. Kn3 Series with C_{60} Absorption Compared to Absorption of C_{60} Alone.

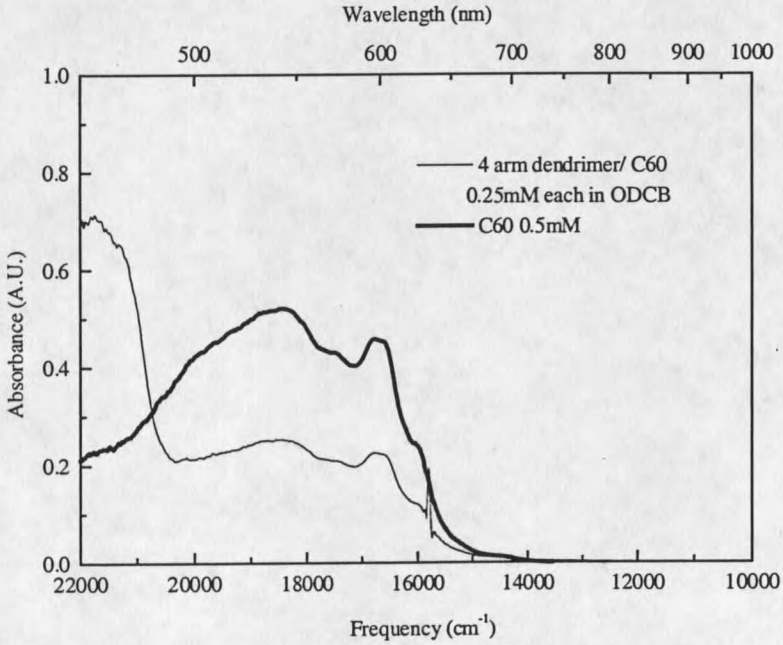

Figure 19. 4 arm Dendrimer with C_{60} Absorption Compared to Absorption of C_{60} Alone.

Species	Absorption @ 532nm	Species	Absorption @ 532nm
Kn1 oligimer/C60	0.4817	Kn3 oligimer/C60	0.9875
Kn1 dendron/C60	0.4353	Kn3 dendron/C60	0.8023
Kn1 dendrimer/C60	0.4709	Kn3 dendrimer/C60	0.6940
Kn2 oligimer/C60	0.4661	4arm dendrimer/C60 0.1mM each	0.1599
Kn2 dendron/C60	0.4497	4arm dendrimer/C60 0.25mM each	0.2721
Kn2 dendrimer/C60	0.5113	4arm dendrimer/C60 0.5mM each	0.5192
		4arm dendrimer/C60 1mM/0.5mM	0.8466

Table 2. Absorption of Tested Species at 532nm. All concentration are 0.5mM each unless otherwise noted. Absorbance is given in absorbance units (A.U.)

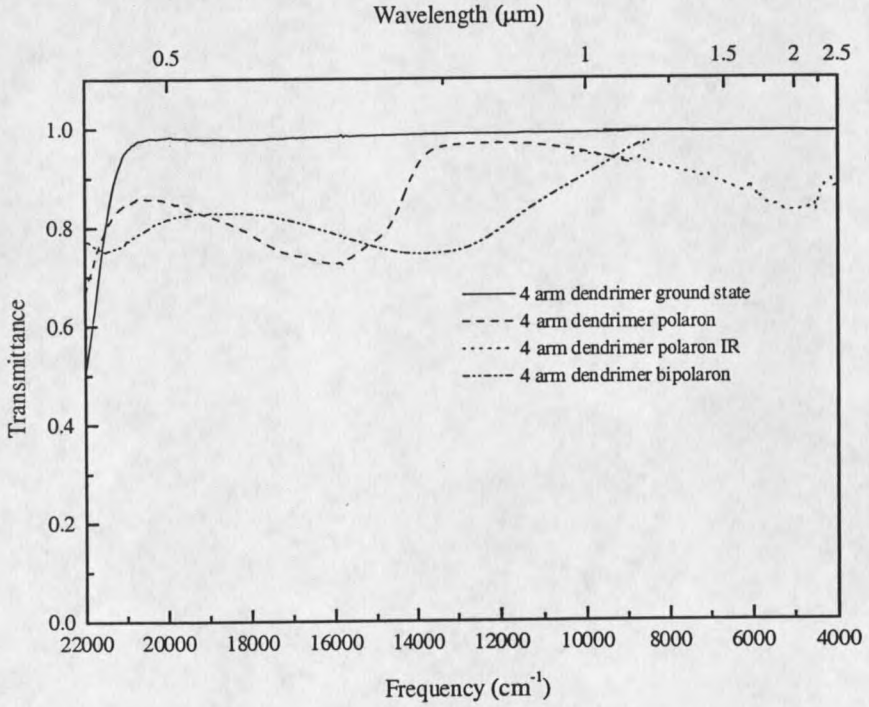

Figure 20. Chemically Induced Absorption Spectra of 4 arm Dendrimer.

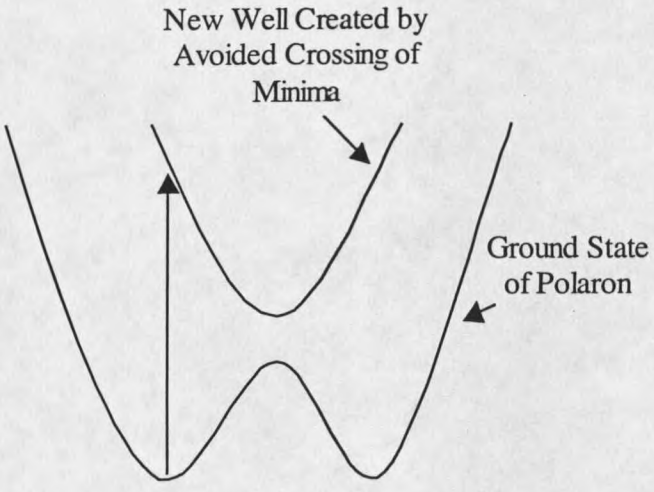

Figure 21. Cross Section of Potential Energy Surface of the Ground State of the Polaron with Two Minima Showing a New Well and Intervalence Transitions Created by an Avoided Crossing.

Absorption of Transient Species

When C_{60} is absorbs light thus promoting an electron to its first excited state, efficient intersystem crossing will leave the molecule in a triplet state. The prescence of this transient species in solution is evidenced by the appearence of a triplet- triplet absorption peak at around 750nm, seen in Figure 22. The time dependance of this absorption gives information about the decay processes of the first C_{60} triplet state.

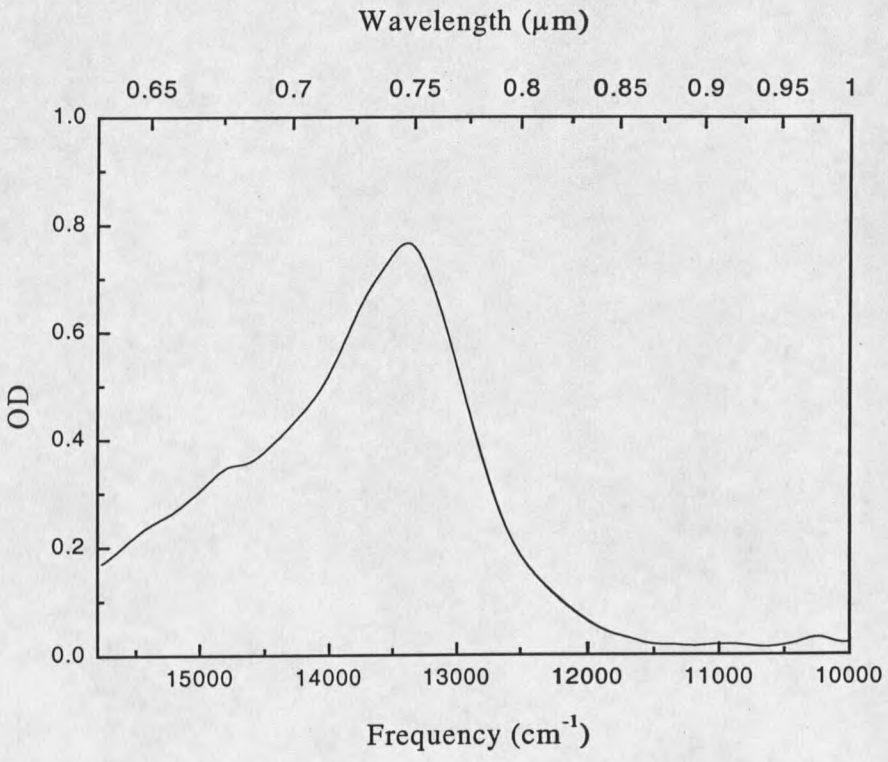

Figure 22. Photo Induced Triplet – Triplet Absorption of C_{60}.

The presence of a photo induced transient species in the 4arm dendrimer /C_{60} solution was first confirmed using the difference method described above. The absorption spans the wavelength of the HeNe reference laser and the filters used to acquire the data on either side of this wavelength have put an artificial "hole" in the spectrum. Figure 23 is uncorrected data, that is the instrument response has not been divided out so the intensity and band shape are not true to life, although they are close. Clearly, this spectrum is not very useful in identifying the transient species, but it does positively affirm the presence of a cooperative effect yielding a new and time dependant species in the solution.

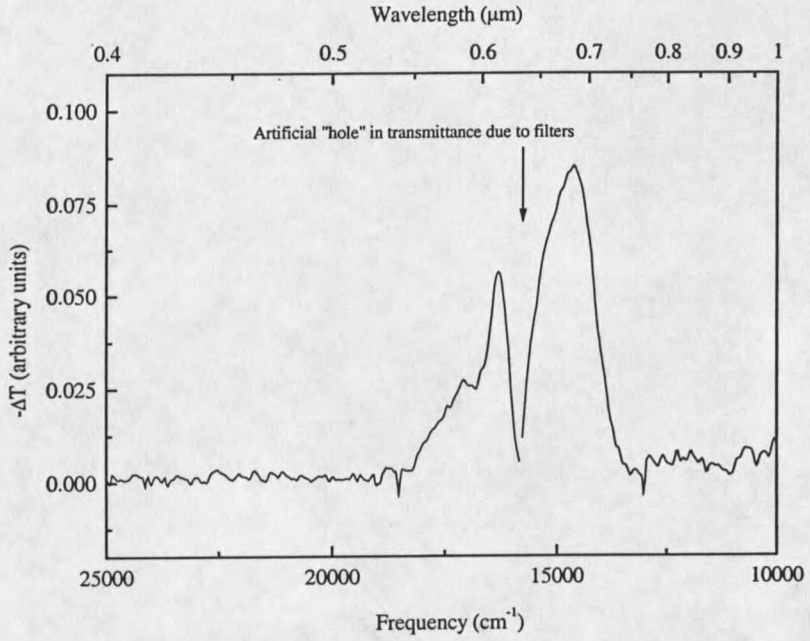

Figure 23. Difference Spectrum of 4 arm Dendrimer/C_{60} Solution. The data has not been divided by the instrument response and the artificial "hole" near 650nm is due to filters. The pump wavelength is 488nm.

Photo-induced activity was identified in the series of molecules with hydroxy substituents using the difference method with an excitation wavelength of 514nm. A distinct shape is seen for each of the chromophores: a more or less single peak for the Kn1 molecule while the Kn2 and Kn3 molecules have three distinct peaks (Figure 24). The absorptions are red shifted with increasing conjugation length as would be expected as the size of the quantum box is increased giving smaller energy spacings. These spectra are qualitatively very similar to the polarons of the original series of chromophores tested for PIA, which is again expected due to the similarity of the structures. Because of this fact, it was concluded that the PIA peaks of Kn1, Kn2 and Kn3 are also due to the

polaron of the chromophores, even without the direct evidence of chemically generated species. Figure 24 gives the PIA bands of only the oligimers. The dendron and dendrimer PIA spectra have the same shape as the oligimer spectrum of the same conjugation length but different intensity.

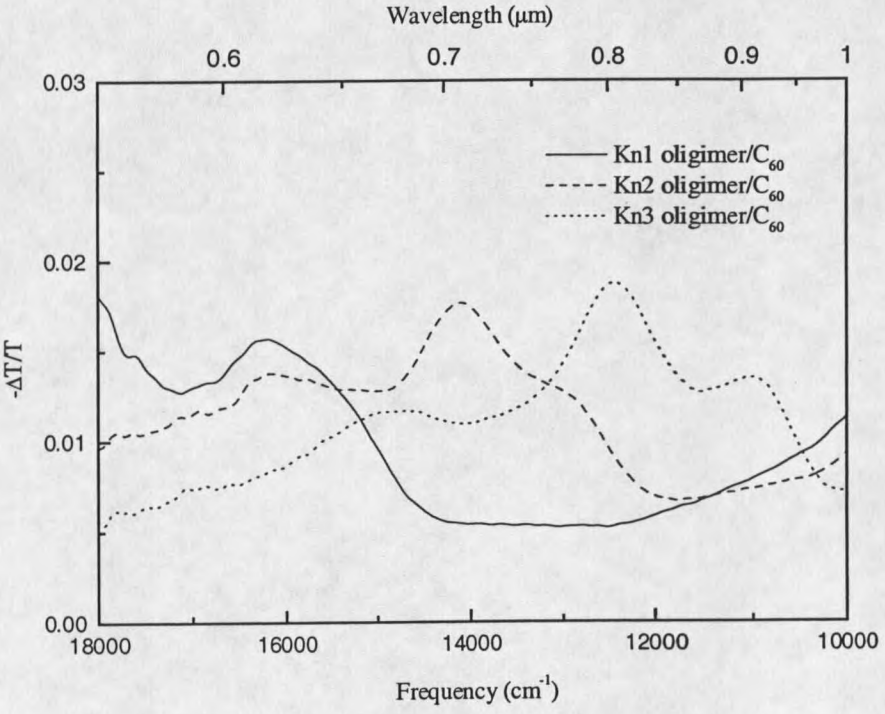

Figure 24. PIA of the Kn1, Kn2 and Kn3 Oligimers with C_{60}. The spectra were taken using the difference method and were pumped at 514nm.

Calculating Rate Constants and Quantum Efficiency

Calculation of the observed rate constants for the forward and reverse electron transfer, and eventually the quantum efficiency, requires that the entire mechanism be broken down into easily modeled parts and examined. Researchers who have examined

photo induced charge transfer of other donor molecules with C_{60} have presented a simple mechanism to describe the behavior of their dilute solution studies which has been adopted here [1,7,8,15-17]. The processes which comprise the electron transfer mechanism and are thus seen in the PIA spectra are described in Scheme 2.

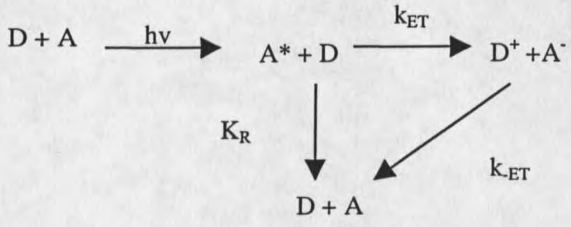

Scheme 2. Mechanism for Charge Transfer Seen in the Molecules Studied. D is the donor, A is the acceptor, k_{ET} is the rate constant of electron transfer, k_{-ET} is the rate constant for back electron transfer and k_R is the rate constant for all other relaxation processes.

Where k_{ET} is the rate of forward electron transfer which includes the rate of diffusion and solvation, k_{-ET} is the rate of back electron transfer, which also includes the rate of diffusion, and k_R is the rate of relaxation of the excited species, this can include radiative and non-radiative means of relaxation, but obviously excludes electron transfer.

The following rate equations apply to the sample after it has been excited by light:

$$\frac{d[A^*]}{dt} = -k_{ET}[A^*][D] - k_r[A^*] \qquad 19$$

$$\frac{d[D^+]}{dt} = k_{ET}[A^*][D] - k_{-ET}[D^-][A^+] \qquad 20$$

In order to extract the concentration values, the optical density of the spectra was calculated. Optical density, OD, is defined as

21

$$OD = -\ln\frac{I}{I_0} = \sum_X \varepsilon_x \ell [X]$$

Where I is the intensity of the light after passing through the sample, I_0 is the initial intensity of the light, ε_x is the molar absorption coefficient of molecule X and l is the path length. A trace of OD versus time was created using the OPUS software. One of three integration methods were employed for this trace generation, each yielding essentially the same results. In the first method, the OD value at a user defined wavelength, usually corresponding to the maximum absorption, was selected. This method was used in regions of the spectrum containing many different absorption peaks and/ or noise. The other method of integration allowed the computer to pick the maximum peak value between two user set wavelengths. A third method that calculated the maximum value of a peak with respect to a baseline, the endpoints of which are selected by the user, was utilized in examining the C_{60} anion decay as this absorption lay on top of the side of the cation absorption for the Kn1 and Kn2 molecules. This method, however, provided for a very noisy time integrated trace for the C_{60} anion.

Time integrated plots were obtained for the IR cation peak of each of the species. Similar plots were drawn for the C_{60} anion and the visible cation peaks but, unfortunately were not useful for several reasons. First, the C_{60} anion peak gave poor signal to noise, as mentioned above. This is possibly due to the presence of a non-linear error in the transmission spectrum which is an artifact of the experimental method. The C_{60} anion absorption lies adjacent to a very sharp absorption attributed to the solvent. This solvent absorption should divide out of the transmission spectrum, as it is present in both I_{pumped} and $I_{unpumped}$, however, due to its very large change in slope, it does not divide completely

accurately and thus leaves an artificial peak or valley at this region. This is possibly a phase correction error and exists whenever these sharp OD changes exist in the spectrum. It is in an unfortunate position with respect to the anion absorption and so this error, coupled with the low concentration of the anion, provide for unusable signal to noise. The molar extinction coefficient for the visible cation peaks is difficult to determine with comfortable accuracy without performing the chemical doping experiments. In addition, there are individual problems with the cation peaks of the different molecules. The peak of the Kn1 and 4 arm dendrimer absorption exist right around the HeNe wavelength and therefore, due to non-linear errors caused by the filters used, it is not easy to get a reliable OD vs. time trace. The Kn2 and Kn3 peaks have problems with early time traces, as the cation peaks are masked by the decay of the C_{60} triplet absorption.

Reverse Electron Transfer

Spectra taken with 5 μsec time resolution examine the behavior of the charge transfer system from 0 - ~500 μsec. The dominate process during this time period is the anion and cation recombination as the forward charge transfer process is complete before the first time slice is recorded (<5 μsec). We can therefore make assumptions which greatly simplify the kinetic analysis of the data. Equation 20, which describes the change in concentration for the cation (or similarly the anion) can be reduced to

$$\frac{d[D^+]}{dt} = -k_{-ET}[A^-][D^+] \qquad 22$$

Notice that $[A^-] = [D^+]$, as one cation is necessarily formed for every anion and therefore the rate equation looks like

$$\frac{d[D^+]}{dt} = -k_{-ET}[D^+]^2 \qquad 23$$

The stoichiometric coefficient is still 1 as there is just one A^- and one D^+ involved in the reaction. The recombination becomes simple to model now as the concentration of anion or cation should follow the relation,

$$\frac{1}{[D^+]_t} = \frac{1}{[D^+]_0} + kt \qquad 24$$

where $[D^+]_t$ and $[D^+]_0$ are the concentration at time t and the initial concentration, respectively. Therefore, a plot of the reciprocal of the concentration versus time should be linear with a slope equal to k_{-ET} and the y intercept equal to the reciprocal of the initial concentration. This was, in fact, the case for most of the molecules studied and extracting the back electron transfer rate was trivial. An example of such a linear fit is given in Figure 25.

Since the OD is directly proportional to concentration with the molar extinction coefficient, ε, as the proportionality term, the slope had to be multiplied by ε in order to generate the actual rate constant. Molar extinction coefficients were calculated by comparing the absorption of one species to another species of the same, or known concentration and known extinction coefficient. In the case of the cations, the values were generated by comparing their absorption at λ_{max} to the absorption of the C_{60} anion, which, it was assumed, has the same concentration. The molar extinction coefficient for the C_{60} anion is reported to be 22,800 M^{-1} cm^{-1} at 1078nm in ODCB [8]. In the case of the Kn1 and Kn2 molecules, the anion peak was on top of the cation peak. In order to find the OD of the anion alone, a base line was drawn underneath the anion peak following

the slope of the cation absorption. OD values were then measured from this line. The calculated values of ε for the IR cations are given in Table 3.

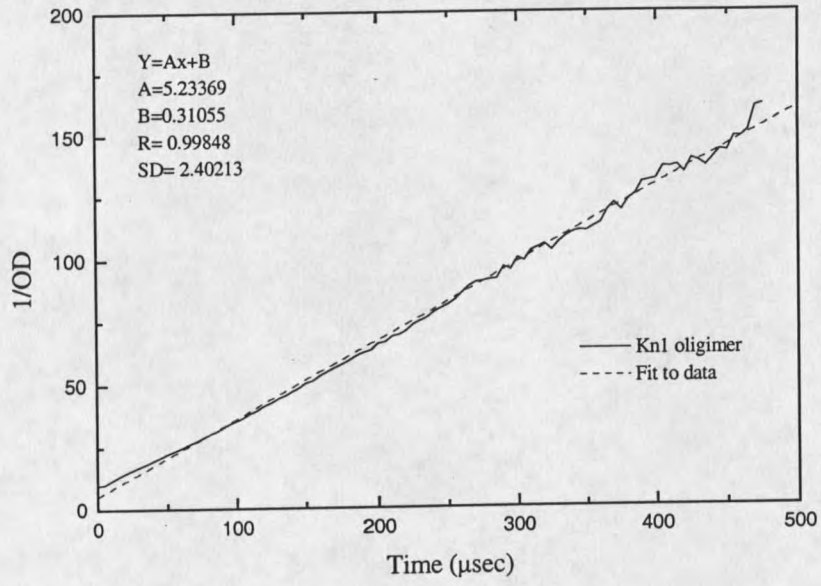

Figure 25. Example of Linear Fit to Reciprocal Optical Density Data.

This method of calculation is not the most ideal method for extracting the molar absorptivities and can introduce significant error if the signal to noise of the spectra is not adequate. In addition, the assumption that the concentration is the same for both species must be valid, which is not always the case between runs (i.e. visible and IR) or at long time if the cation and anion decay by different paths. Every effort was made to generate believable values, but the difference in molar absorptivity values calculated between different experimental runs was sometimes uncomfortably large. Additionally, there does not seem to be a general pattern among the molecular series with respect to the molecule

and the absorptivity coefficient and the Kn2 values are significantly lower than the others. This was the best way available to extract these values and the maximum error is around 20%.

Compound	Molar extinction coefficient (M^{-1} cm^{-1})
Kn1 oligimer	68000
Kn1 dendron	89000
Kn1 dendrimer	90000
Kn2 oligimer	37000
Kn2 dendron	32000
Kn2 dendrimer	33000
Kn3 oligimer	104000
Kn3 dendron	115000
Kn3 dendrimer	136000
4 arm dendrimer (visible cation)	67000

Table 3. Molar Extinction Coefficients of the Polarons of the Molecules Studied.

The 4 arm dendrimer was treated a little differently due to the position of its IR cation absorption at the far edge of the detection region. Because of this and the solvent generated non-linearities near its maximum wavelength position, reliable time traces were not possible for the 50nsec time resolution experiments. Therefore, the visible cation peak was used. In order to calculate the molar absorptivity of the visible peak, it was first necessary to find that of the IR peak by equating it to the C_{60} anion absorption. Spectra taken using the 5 μsec time resolution were used for this relation because they had better signal to noise. After this was achieved, the IR and visible absorptions of the

chemically induced polaron were compared to yield the molar extinction coefficient of the visible cation peak reported.

It was mentioned before that most of the compounds displayed a linear dependence on 1/[X], this is not the case for the Kn2 dendrimer and the Kn3 dendron and dendrimer. Each of these plots displays varying degrees of curvature, as evidenced by Figures 26-28. Some curvature in the intensity versus time plots has been seen before in emission studies using the interferometer. The effect occurs in the time traces of smaller magnitude peaks when a more intense emission band is present in the same sampling region and appears to be due to problems in baseline correction. Additionally, this curvature seemed to be very gradual over the course of time. This being the case, a small amount of non-linearity can be accounted for, however, the degree of curvature seen in these plots is outside what is attributable to this artifact, especially in the case of the Kn3 dendrimer, and indicates that there is additional decay process that needs to be considered.

In the cases where this type of curvature is seen, a linear fit was applied to two independent regions of the trace, one at early time and one at later time. The rate constants generated by the fit at early time correlate well with those seen in the other molecules while the rate constants for later time are smaller. The average values of the rate constants calculated for each of the molecules is given in Table 4 and Figures 29-31 display the calculated rate constants for several different experimental runs, showing the typical level of dispersion.

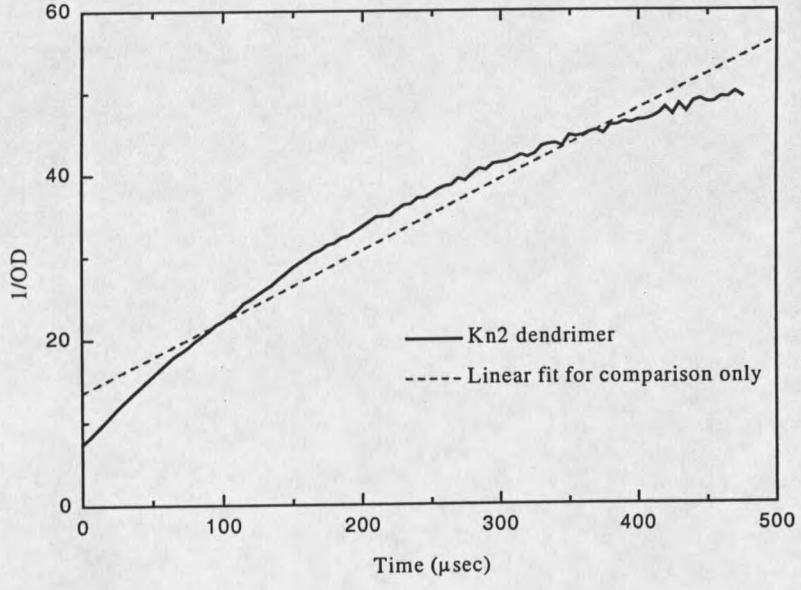

Figure 26. Kn2 Dendrimer Decay Curve with Linear Fit for Comparison.

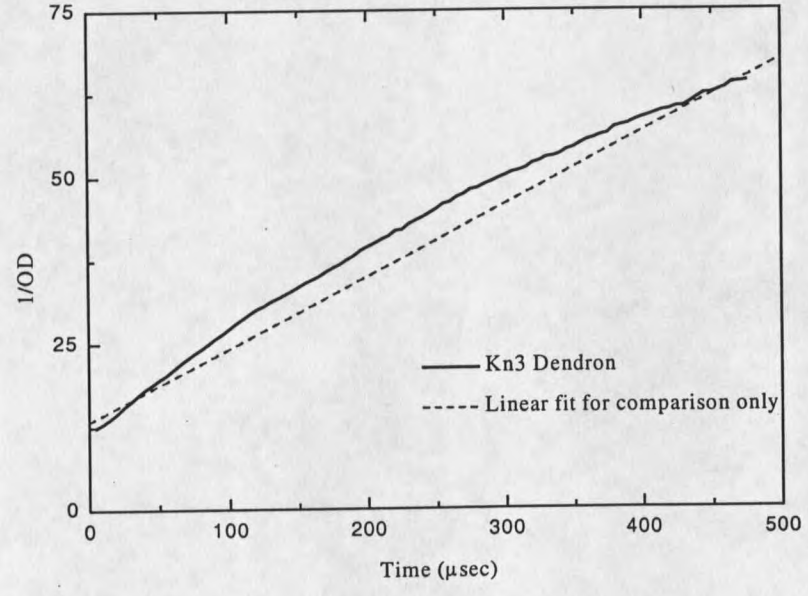

Figure 27. Kn3 Dendron Decay Curve with Linear Fit for Comparison.

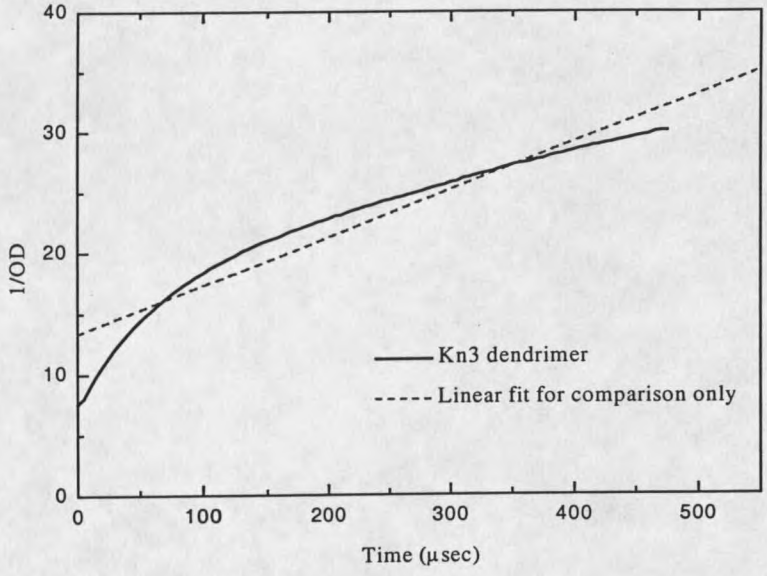

Figure 28. Kn3 Dendrimer Decay Curve with Linear Fit for comparison.

Compound	Average Recombination rate constant (k_{-ET}) (L/mol s)	Percent Standard Deviation
Kn1 oligimer	2.5×10^{10}	18%
Kn1 dendron	2.2×10^{10}	10%
Kn1 dendrimer	1.9×10^{10}	23%
Kn2 oligimer	7.8×10^{9}	11%
Kn2 dendron	5.6×10^{9}	14%
Kn2 dendrimer	4.1×10^{9} (early) 3.5×10^{9} (late)	5% (early) 19% (late)
Kn3 oligimer	1.6×10^{10}	18%
Kn3 dendron	1.7×10^{10} (early) 7.8×10^{9} (late)	5% (early) 30% (late)
Kn3 dendrimer	1.4×10^{10} (early) 3.8×10^{9} (late)	10% (early) 5% (late)
4 arm dendrimer 0.1mM each	2×10^{10}	10%
4 arm dendrimer 0.25 mM each	3×10^{10}	21%
4 arm dendrimer 0.5mM each	2×10^{10}	8%
4 arm dendrimer 1mM/0.5mM	2×10^{10}	13%

Table 4. Average Recombination Rate Constant, k_{-ET}, for the Molecules Studied with C_{60}.

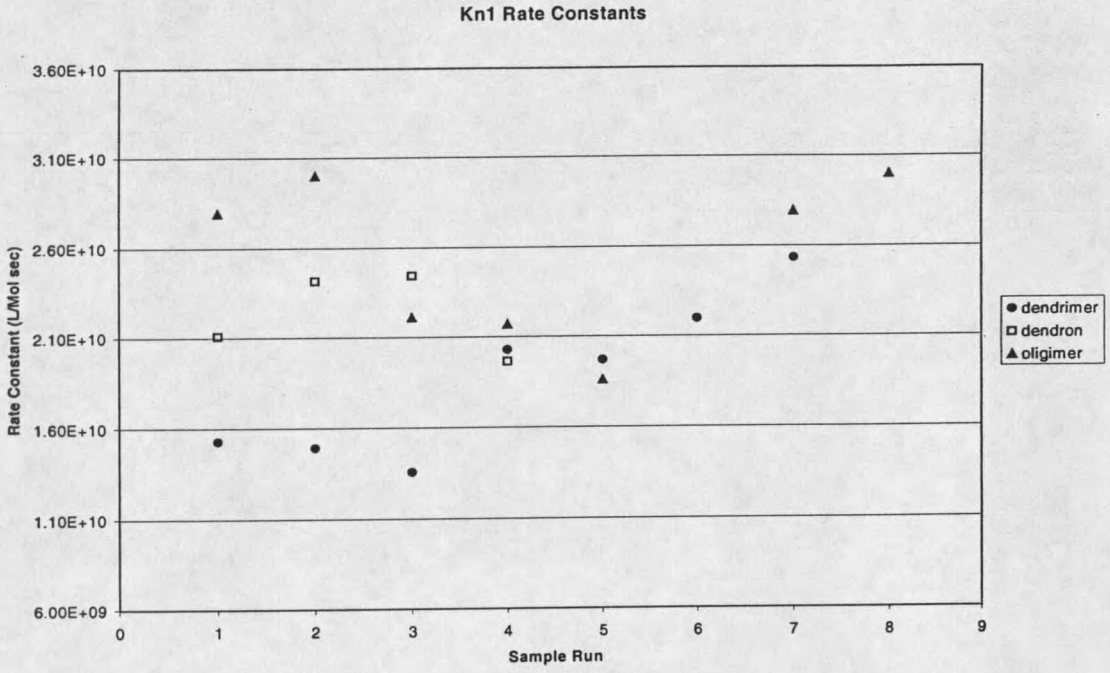

Figure 29. Calculated Recombination Rate Constants, k_{-ET}, for Kn1 Series with C_{60}.

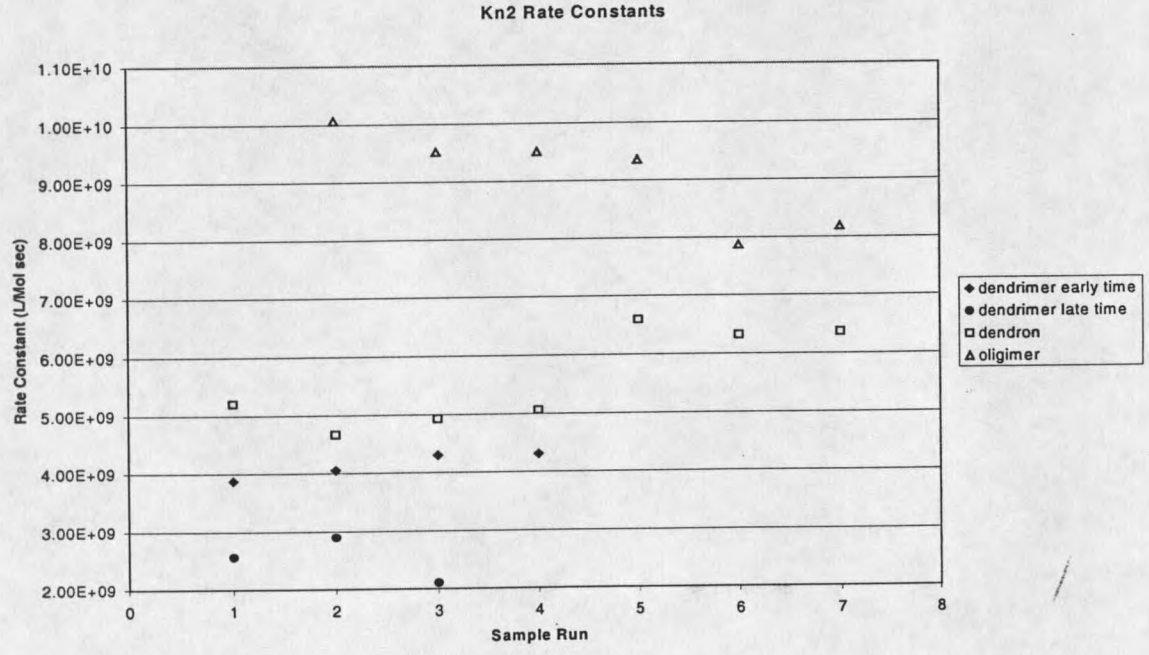

Figure 30. Calculated Recombination Rate Constants, k_{-ET}, for Kn2 Series with C_{60}.

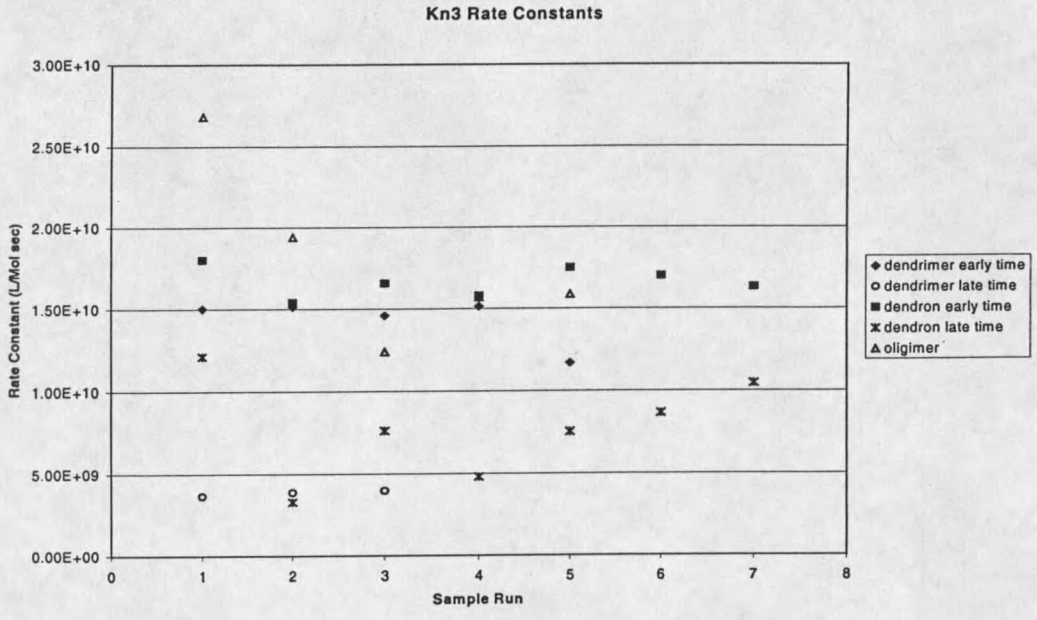

Figure 31. Calculated Recombination Rate Constants, k_{-ET}, for Kn3 Series with C_{60}.

These values are very close to the example of a diffusion limited rate constant cited before, 6×10^9 L/mol sec [6]. The slightly larger values reported here are to be expected due to two issues. The example rate constant is calculated for neutral molecules of 2×10^{-8} cm radius in water [6], where as the experimental rate constants are for slightly larger, oppositely charged ions in ODCB, which has similar viscosity and a dielectric constant of approximately one order of magnitude less. The major contributor to this difference seems to be the coulombic effects brought about by the presence of a cation and anion in close proximity. Such a change in charge can easily increase the rate constant by a factor of 2, as mentioned previously. The rate constants tend to decrease with an increase in size, although only slightly. In addition, the rate constant of the 4 arm dendrimer stays more or less constant with concentration, as it should. The value for the

0.25mM solution is, however, anomoulously high and it should be noted that the data runs for this molecule had a larger standard deviation than the others. To be appropriately thorough, more data should be taken and analyzed at this concentration in the future.

The presence of two rather distinct regions of more or less linear behavior with respect to 1/[X] and similar but different rate constants can possibly be explained by two second order recombination processes that are both diffusion limited. The first is obviously cation – anion recombination and the second is a radical cation – radical cation reaction. The latter pathway should produce a completely different molecule which, depending on its stability, could be detected and characterized, which would support this theory. This has not been performed at this time, however there are other considerations which provide some basis for this theory. Such a reaction pathway has been considered by Witgens et al. in systems of thiophene oligimers [18]. The order of magnitude of the rate constant indicates a diffusion limited process, so it is not a reaction with the solvent, leaving only anions, cations, neutral molecules or a possible impurity as candidates. It is believed that the process is linear with 1/[X] and therefore is either an A^2 -> B type reaction or an A + B -> C type reaction where A and B are of the same concentration. The latter possibility includes the cation-anion reaction and the former, a radical cation-radical cation reaction. Reactions of the cation with neutral molecules or an impurity would be second order in two different species or pseudo-first order and therefore would not have the same temporal behavior as is witnessed. In addition, due to the repulsion of like charges, a diffusion limited cation- cation reaction would be expected to be slower than even neutrals in solution. The rate constants would in fact be half of what is reported

if this is an A^2 -> B type reaction due to the stoichiometric coefficient and therefore smaller than the diffusion limited rate constants of the neutral molecules which will be reported later. They are, in fact, approximately the same as or slightly smaller than these values. If such a reaction was occurring then it is expected that the decay curve of the cation and anion of these molecules would behave differently. This has unfortunately not been examined due to the aforementioned problem with the anion absorption. Of course, it must be considered why such a reaction only appears to occur appreciably in the Kn2 dendrimer and Kn3 dendron and dendrimer. It is possible that the additional stability of these larger molecules due to increased conjugation and possibly the stability of the products makes this a favorable route for the decrease in cation population.

It is perhaps too strict to say that there are two linear regions in these plots and it is possible that the kinetics follows some other mechanism that is not linear with 1/[X]. In this case, there are more mechanisms that would explain these decays than what has been argued here, processes that involve the neutral molecules, for instance. A notable possibility in this category, which would also have a small rate constant, is the presence of two charged species on one molecule. Each of the chromophores on the dendron and dendrimer has been shown to absorb light as if it were independent of the others through absorption and doping studies performed by Kimba Ashworth[10]. It is cerainly possible that a dendron or dendrimer molecule could have more than one charged arm and that each of these polaron arms would have the same absorption as a single polaron by itself. This one donor molecule would then have to encounter two acceptor ions to become neutral, giving more complex kinetics and a smaller rate constant. However, the

probability that two arms on one molecule would be oxidized by separate $^3C_{60}$ molecules is around 1 in 100, therefore the concentration of these species would be on the order of 1×10^8 M and not large enough to play such a large role in the kinetics.

Forward Electron Transfer

Spectra taken at 50nsec time resolution focus on forward electron transfer and additional relaxation processes of the C_{60} triplet state and also gives some information about back electron transfer. The OD versus time traces of the cations show a rise and decay of the transient after laser excitation. These two processes are most easily treated separately as the kinetics involved to fit the whole curve become quite complicated. It is within the scope of the assumptions already made to plot the decay seen in these traces just as the 5 μsec resolution data. In fact, the traces are linear with 1/[X] and the rates correlate quite well, especially with the early time data for the Kn2 dendron and Kn3 dendron and dendrimer.

The rise is difficult to fit as there are very few data points that can be attributed to the rise only. Moving to a faster temporal regime or slowing down the reaction will be necessary to get conclusive fits to this process. The decay of the triplet – triplet absorption, on the other hand, has good signal to noise and is fairly easy to fit. The rate equation for the triplet state is,

$$\frac{dA^*}{dt} = -k_R[A^*] - k_{ET}[A^*][D] \qquad 25$$

In order to simplify the equation, it can be assumed that the concentration of the donor molecules will not change significantly over time and thus the second term of the right

hand side of the equation reduces to a pseudo-first order process. This assumption can be evaluated later, for now it provides a good place to start. After integrating and simplifying, the time dependence becomes,

$$[A^*]_t = [A^*]_0 \exp[-(k_R + k_{ET}[D])t] \qquad 26$$

A plot of OD versus time should be exponential with a coefficient equal to the sum of the rate constants of the decay processes and a pre-exponential factor equal to the initial concentration of the triplet, after dividing by the molar absorptivity. This value in ODCB is not actually given in the literature, however it is reported to be 15,000 M^{-1} cm^{-1} in toluene [19], 16,000 M^{-1} cm^{-1} in benzonitrile [16] and the C_{60} dimer is reported to be 14,000 M^{-1} cm^{-1} in ODCB [20] at the wavelegth of maximum absorbance, ~750nm , therefore an average value of 15,000 M^{-1} cm^{-1} is used. Such traces were generated and fit with a linear regression on a semi-log plot. This was straightforward for the Kn1 molecules and the 4arm dendrimer because the visible cation absorption is sufficiently separated from the triplet- triplet absorption. For the Kn2 and Kn3 molecules, this was not the case and so the rise of these cations had to be subtracted from the triplet decay trace. This was achieved by using the temporal trace of the IR cation normalized to the molar absorption coefficient of the visible peak at the sampled wavelength.

The rate constant for electron transfer can be extracted from this observed rate constant by finding the value of k_R. This is achieved by looking at the PIA of C_{60} alone in solution and fitting this first order process in the same fashion as above. A rate constant of 9.6 x 10^5 sec^{-1} was observed. After this number is subtracted from the $k_R + k_{ET}[D]$ values generated from the acceptor donor systems, and the concentration of the donor

molecule at 0.5 mM is removed, a rate constant for forward electron transfer remains. The average rate constants for the compounds studied are given in Table 5.

Compound	Average Forward electron transfer rate constant (k_{ET}) (L/mol sec)	Percent Standard Deviation
Kn1 oligimer	2.1×10^9	4%
Kn1 dendron	3.4×10^9	7%
Kn1 dendrimer	3.9×10^9	6%
Kn2 oligimer	1.7×10^9	1%
Kn2 dendron	4.0×10^9	2%
Kn2 dendrimer	5.0×10^9	2%
Kn3 oligimer	7.8×10^8	10%
Kn3 dendron	1.0×10^9	19%
Kn3 denrimer	1.2×10^9	10%
4 arm dendrimer 0.1mM each	2.0×10^9	*
4 arm dendrimer 0.25 mM each	*	*
4 arm dendrimer 0.5 mM each	1.9×10^9	1%
4 arm dendrimer 1/0.5 mM	3.0×10^9	4%

Table 5. Average Forward Electron Transfer Rate Constants for Molecules Studied with C_{60}. *This rate constant requires more analysis.

It is interesting that the rate constant increases slightly from oligimer to dendrimer, although the change is for the most part small, about a factor of two. This difference can possibly be attributed to the larger radius of the molecules, the alleviation of orientation restraints or a smaller solvent reorganization energy. As expected, the rate constant for the 4 arm dendrimer is approximately the same no matter what the

concentration, the higher concentration value is slightly higher, and it is unclear why. Unfortunately, inadequate data was taken for a conclusive evaluation of the 0.25mM solution.

The values are all slightly lower than the diffusion limited rate constant calculated for water. However, that figure is just a guideline and the fact that these numbers are of the same order of magnitude is encouraging. Actual values expected for diffusion limited rate constants in ODCB with experimental molecules are hard to calculate because diffusion coefficients and molecular radii are difficult to obtain for molecules that have not been studied in depth and approximations give more or less an order of magnitude result. There is significant confidence in the statement that the triplet quenching process is diffusion limited.

Quantum Efficiency

When all of the hypothesized rate constants have been calculated it is beneficial to look at the quantum efficiency of the forward electron transfer process. This value will give an idea of how useful the donor /acceptor system will potentially be in an optical limiting arrangement. The ratio of charged states that are actually generated to give RSA compared to those that could be produced, in this case one ion pair for every C_{60} triplet is the maximum, should be as great as possible. The quantum efficiency of electron transfer in this system, Φ, is just the rate of charge state formation divided by the sum of all of the de-excitation pathways,

$$\Phi = \frac{k_{ET}[D]}{k_R + k_{ET}[D]} \qquad 27$$

There are three ways to calculate this value. The first is to simply plug the calculated rate constants in to the above equation. Doing so yields unexpectedly high, but encouraging, quantum efficiencies that are listed in Table 6.

Compound	Quantum Efficiency
Kn1 oligimer	52%
Kn1 dendron	64%
Kn1 dendrimer	67%
Kn2 oligimer	64%
Kn2 dendron	67%
Kn2 dendrimer	72%
Kn3 oligimer	29%
Kn3 dendron	35%
Kn3 dendrimer	38%
4 arm dendrimer 0.1mM each	13%
4 arm dendrimer 0.25mM each	*
4 arm dendrimer 0.5mM each	50%
4 arm dendrimer 1/0.5 mM	76%

Table 6. Quantum Efficiency for Molecules Studied Using Calculated Rate Constants. *This rate constant requires more analysis.

There is a general increase in the quantum efficiency as the size and number of chromophores on a molecule grows or as the concentration is increased. This was a hoped for result and is one of the reasons behind the synthesis of the dendrimers. However, the difference is not large and may not justify the added complication of

dendron and dendrimer synthesis. This is especially true when coupled with the fact that there is not a large change in rate constant with the dendrons and dendrimers, as was originally hypothesized. It was thought that the increased conjugation and potential for two dimensional delocalization would make the polaron and/or bipolaron of the dendron and dendrimer considerably more favorable and thus better for limiting applications.

Such large quantum efficiency values were at first startling based on the rough calculations of the original bis-(diphenylamino) diphenylpolyene series via other calculation methods. The concentrations of cations and triplet produced in each of the systems also pointed to lower values. As a quick check, the integrated areas underneath the triplet decay curves of the donor-acceptor system and the acceptor alone were compared. This ratio confirmed the numbers calculated above.

The second method is to calculate the ratio $[D^+]_{max}/[A^*]_{max}$ (or similarly $[A^-]_{max}/[A^*]_{max}$). The cation peaks had better signal to noise, so they were used to evaluate this quotient. Temporal traces with 50ns resolution were used and the maximum value of the IR cation absorption was extracted (except for the 4 arm dendrimer where the visible cation absorption was used). The optical density for the triplet – triplet absorption was taken from the trace of the C_{60} alone in solution at 0.5mM. It was assumed that a comparable number of C_{60} molecules in the donor- acceptor solutions would be excited to the triplet state. The values were not extracted from the C_{60} /chromophore systems because quenching of the triplet state had already occurred by the first time slice giving a deceptively lower initial triplet concentration value. The concentrations and quantum yields for each molecule are listed in Table 7.

Compound	Concentration of transient	Quantum Yield	Percent Standard Deviation
Kn1 oligimer	1.5×10^{-6} M	2%	1%
Kn1 dendron	1.9×10^{-6} M	2.5%	
Kn1 dendrimer	1.1×10^{-6} M	1%	5%
Kn2 oligimer	4.4×10^{-6} M	6%	7%
Kn2 dendron	8.2×10^{-6} M	11%	5%
Kn2 dendrimer	9.0×10^{-6} M	12%	2%
Kn3 oligimer	8.8×10^{-7} M	1%	10%
Kn3 dendron	5.5×10^{-7} M	1%	17%
Kn3 dendrimer	3.8×10^{-7} M	0.5%	2%
4 arm dendrimer 0.5mM	6.8×10^{-6} M	10%	4%
4 arm dendrimer 1/0.5mM	1.3×10^{-5} M	15%	4%
C_{60} Triplet	7.5×10^{-5} M		

Table 7. Concentrations and Quantum Yields Calculated using $[D^+]_{max}$ and $[A^*]_{max}$ Values.

A comparison between these quantum efficiency values and those calculated using the rates shows a very large discrepancy. These values are significantly smaller and the efficiency is more or less the same for all of the molecules in a series. More discussion of this phenomenon will follow. It would appear that the Kn2 series and the 4 arm dendrimer are the most efficient molecules. However, the very low molar absorptivities of the Kn2 series, as mentioned above, make these values suspicious. It is not known why these molecules appear to perform better and certainly warrants more consideration and investigation. The quantum efficiency of the 0.1mM and 0.25mM 4 arm dendrimer/ C_{60} solutions was not calculated because the C_{60} alone triplet information was run at a concentration of 0.5mM only.

This second method of calculating electron transfer quantum efficiency from maximum values is generally used by researchers, however, it neglects the effects of back charge transfer by ion recombination, which can become appreciable, especially as the ion concentration builds. The third way to calculate quantum efficiency, developed in this research group, de-couples the effect of back charge transfer from the calculation of quantum yield, at least at early time [21]. It requires the presence of an isobestic (isoabsorptive) point in the data, where one species is gaining population at the expense of another.

If the absorption present in the region of the isobestic point is only due to the transient species involved, the OD can be defined as,

$$OD = -\ln\frac{I_P}{I_U} = \left(\varepsilon_{A^*}[A^*] + \varepsilon_{D^+}[D^+]\right)\ell \qquad 28$$

Where I_p and I_u are the intensity of the light when the laser pulse is present (pumped) and not present (unpumped), respectively. The time derivative of the OD is,

$$\frac{dOD}{dt} = \left(\varepsilon_{A^*}\frac{d[A^*]}{dt} + \varepsilon_{D^+}\frac{d[D^+]}{dt}\right)\ell \qquad 29$$

Using the rate equations defined above (equations 19 and 20), equation 29 can be written as,

$$\frac{dOD}{dt} = \varepsilon_{A^*}\left(-k_r[A^*] - k_{ET}[D][A^*]\right) + \varepsilon_{D^+}\left(k_{ET}[A^*][D] - k_{-ET}[A^-][D^+]\right)\ell \qquad 30$$

Simplifying this expression gives,

$$\frac{dOD}{dt} = k_{ET}[A^*][D]\left\{-\frac{\varepsilon_{A^*}}{\Phi} + \varepsilon_{D+} - \varepsilon_{D+}\frac{k_{-ET}[A^-][D^+]}{k_{ET}[A^*][D]}\right\}\ell \qquad 31$$

At the wavelength of the isobestic point, λ_i , dOD/dt = 0 and so either

$$-k_{ET}[A^*][D] = 0 \qquad 32a$$

or

$$\frac{\varepsilon_{*A}(\lambda_i)}{\Phi} - \varepsilon_{D^+}(\lambda_i) + \varepsilon_{D^+}(\lambda_i)\frac{k_{-ET}[A^-][D^+]}{k_{ET}[A^*][D]} = 0 \qquad 32b$$

The first statement cannot be the case and so the following conclusion can be drawn,

$$\frac{\varepsilon_{A^*}(\lambda_i)}{\varepsilon_{D+}(\lambda_i)} = \Phi\left\{1 - \frac{k_{-ET}[A^-][D^+]}{k_{ET}[A^*][D]}\right\} \qquad 33$$

At early time (t < ~1μsec), $[A^*][D] >> [A^-][D^+]$ and so

$$\frac{\varepsilon_{A^*}(\lambda_i)}{\varepsilon_{D+}(\lambda_i)} = \Phi \qquad 34$$

Therefore, the quantum efficiency of the charge transfer process at early time can be calculated by comparing the molar absorptivities of the transient species at the isobestic point.

Only one of the groups of molecules, Kn3, exhibited an isobestic point in the detectable region, seen in Figure 32. The wavelength of the isoabsorptive point was noted for several time traces after the first usable spectrum. The first usable spectrum unfortunately occurs about 350 ns after the laser has excited the sample, this is due to emission from the Kn3 species which saturates the detector and overshadows the PIA. Therefore, a significant amount of early time data is lost, however, quantum efficiencies can still be calculated as long as the isobestic point remains more or less in one spot.

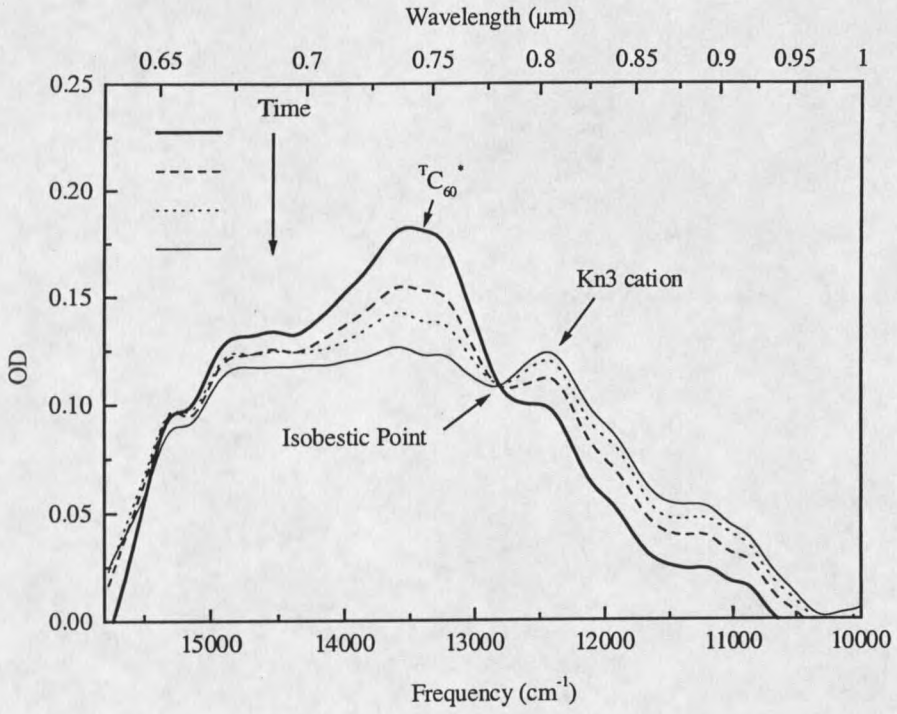

Figure 32. Example of the Isobestic Point in Kn3 Molecules.

The cross point was determined by comparing the wavelength of overlap of a trace at time=t with the one at time = 0, where time = 0 corresponds to 350ns, in this case. The molar absorptivity at this wavelength of the C_{60} triplet and the cation was extracted from the C_{60} alone PIA and the PIA of the respective cation at long time, when it could be assured that there was no triplet- triplet absorption contributing to the spectrum. This was achieved by comparing the OD at this wavelength to the OD at λ_{max} and ratioing the molar extinction coefficients. These numbers were then divided to give the quantum yields reported in Figure 33.

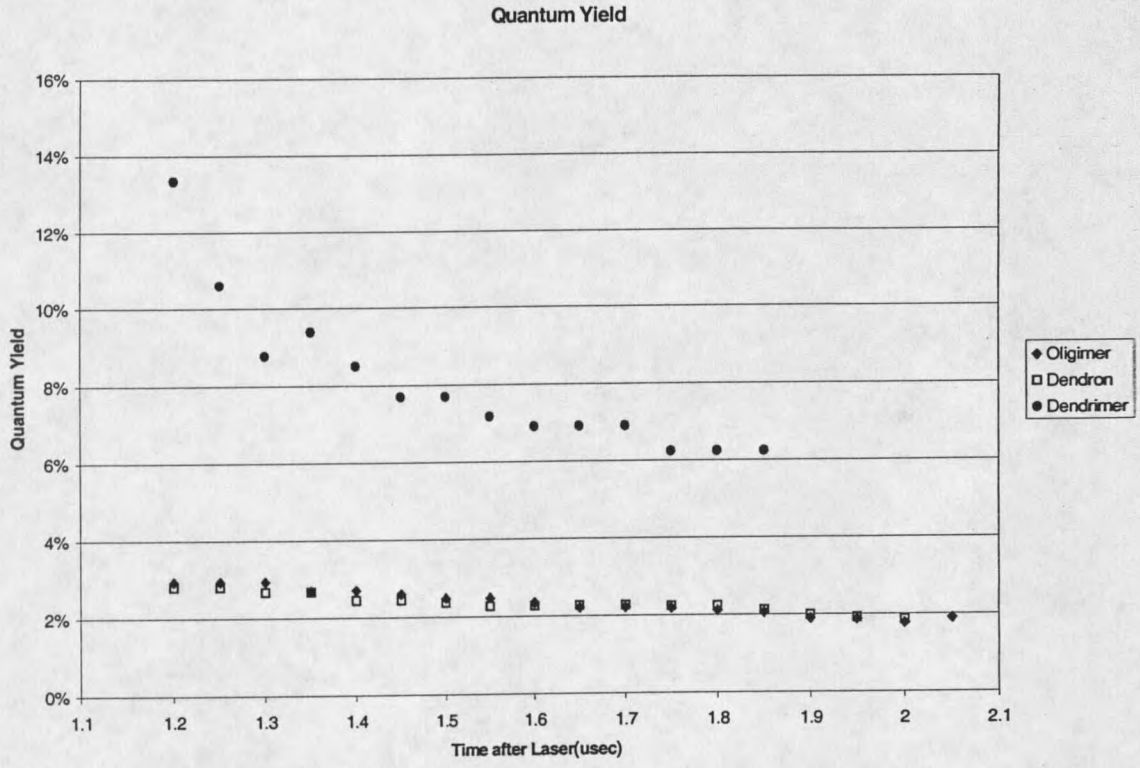

Figure 33. Quantum Yield Efficiencies Calculated Using Isobestic Point method.

The noticeable decrease in the quantum efficiency of the dendrimer with time indicates that reverse charge transfer is becoming a major factor in the size of the absorption peak. The assumption that the ion population is insignificant can no longer be made and the quantum efficiency of merely the forward charge transfer can no longer be calculated in this way. The assumption appears to apply for the oligimer and the dendron, on the other hand, as their efficiency remains more or less constant over this time period. These numbers are again curious when compared to the quantum efficiency values already calculated. The percentage for the oligimer and dendron is similar to those generated by comparing maximum concentrations, however. The dendrimer yield is

approaching those values after starting off at a level similar to, yet still lower than, the quantum yield values calculated by comparing the rates. The question at this point is, of course, why are these quantum efficiencies so different? The answer lies in a re-evaluation of process and the assumptions already made. The first method of calculating quantum efficiencies, using the rates now defined as k_{ET} and k_R , is actually looking at just the quenching of the triplet state. It has been assumed that the only process that is depopulating the triplet state, in addition to "normal" relaxation processes, is charge transfer and that all of these ions are solvated. The second method gives a ratio between those ions that are created and actually solvated and the triplet population. If recombination of the solvated ions is fast, this value may be lower than it should be. The third method also measures the ratio of solvated ions to the number of C_{60} molecules in the triplet state, however, it returns a value that does not include the effect of the back electron transfer process on the concentraion of solvated ions and thus may give more useful values. The discrepancy in the efficiencies can be explained if electron transfer resulting in solvated ions is not the only quenching path. There are several possible pathways that should be considered: 1) energy transfer resulting in heat or some similar loss mechanism; 2) energy transfer resulting in D^* and 3) electron transfer followed by geminate recombination before solvation can occur. The first possibility seems unlikely due to the dependence of the quenching on the presence of the donor molecules. Collisional thermal energy loss should occur with any molecular partner including the solvent. The addition of a relatively small amount of donor should not have such a large effect and therefore this is not likely the quenching mechanism. The second pathway is

dependent on the relative energies of the C_{60} and donor triplet states. In all cases, the singlet state of the donor is higher in energy than the singlet of the C_{60}. If this is also true of the triplet states then energy transfer will not occur. If energy transfer is prevalent, emission may be detectable. However, it is quite likely that relaxation would occur via a non-radiative pathway based on the density of states of the solvent vibrations available to the molecule. Looking at the rise of the ion peaks would be very useful in elucidating the quenching process as the rise of the absorption would give an indication of the rate constant encompassing k_{ET} and $k_{solvation}$. Discrepancies between the rise of the ions and the decay of the triplet can give more information as to the magnitude of the competing processes. With this information in mind, a slightly modified mechanism for the cooperative processes in these systems in proposed. Such a mechanism is discussed by several authors who have been performing experiments in the picosecond time regime where the absorption and emission of geminate ion pairs can be detected or who are working with ground and excited state charge transfer complexes [22-26]. In this mechanism, the different possible triplet quenching processes are distinguished and a geminate ion pair is introduced as an intermediate in the electron transfer process. The nature of this ion pair is discussed in some detail by the above authors [22-25] who introduce the concept of a contact radical ion pair (CRIP) and a solvent separated radical ion pair (SSRIP). These species have slightly different forward electron transfer and decay behaviors and rates. These differences lie outside of the scope of this thesis but are of significant interest to the L. Spangler research group as they proceed toward picosecond time resolved spectroscopy.

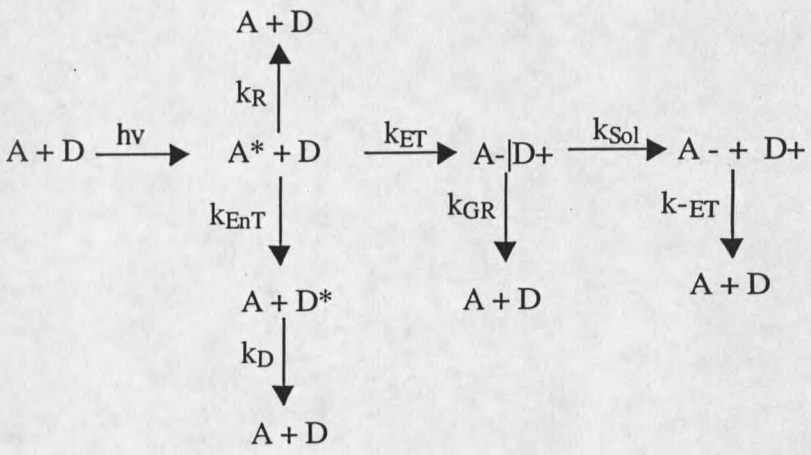

Scheme 3. Modified Mechanism for the Cooperative Processes Present in the Molecular Combinations Studied. k_R is the "natural" relaxation of the triplet, k_{ET} is the rate constant for electron transfer k_{EnT} is the rate constant for energy transfer, k_D is the rate constant for the decay of the excited donor, k_{GR} is the rate constant for geminate recombination, k_{Sol} is the rate constant for solvation and k_{-ET} is the rate of back electron transfer via solvated ion recombination. A-|D+ is a geminate ion pair

Example rate constants corresponding to this mechanism taken from the values calculated for the Kn1 oligimer as well as example rate constants taken from the literature are given in Table 8. k_Q in the table includes the rate constants for electron transfer followed by geminate recombination and energy transfer followed by relaxation of the excited donor molecule. The literature values reported are for various different donor acceptor systems and solvents (those in ODCB are noted) and are all experimentally determined unless otherwise listed. Importantly, it is clear that the rate constants calculated in this thesis fall comfortably within the reported ranges.

Rate Constant	Value from thesis	Value from literatrure
k_Q	2.1×10^9 L/mol sec	$6.4 \times 10^9 - 1.2 \times 10^{10}$ sec^{-1} [17] 5.7×10^9 L/mol sec in ODCB [8]
k_{GR}		~1 x 10^8 - ~1 x 10^{10} sec^{-1} [22]
k_R	9.6×10^5 sec^{-1}	
k_{-ET}	1.5×10^{10} L/mol sec	$0.9 \times 10^7 - >10^8$ sec^{-1} [26] $1.5 \times 10^7 - 4.3 \times 10^9$ sec^{-1}(calculated) [26] $5 \times 10^8 - 1 \times 10^9$ sec^{-1} [22] $7.5 \times 10^9 - 2.6 \times 10^{10}$ L/mol sec (experimental and calculated) [17] 4×10^{10} L/mol sec in ODCB [8]

Table 8. Example Rate Constants for the Mechanism in Scheme 3. k_Q includes k_{ET} followed by k_{GR} and k_{EnT} followed by k_R. Literature values are for different donor acceptor systems in various solvents.

In order to simplify equations involved in fitting the triplet decay in the donor-acceptor solutions, it was assumed that the donor concentration did not change significantly with time. This justified an exponential fit to the data, which seemed to work well, generating fits of good agreement. However, this would not be the case if too many donors wound up as cations in solution, with 10% as the absolute maximum comfort level. Quantum efficiencies measuring this show only a few percent yield on this process, so the original assumption seems sound. On the other hand, the quenching efficiencies do not support such a simplification at first glance, even though the model works quite well with the data. This can be explained based on the proposed quenching mechanisms. In the case of electron transfer followed by geminate recombination, the process is assumed to be very fast and thus justifies a steady state approximation of the

rate of change of the donor concentration. Therefore, the quenched decay of the triplet would still be exponential. The same is perhaps true for an energy transfer process, although this would have to occur with the triplet state of the donor molecules as the singlet state is too high in energy. The triplet state decay should be fairly long lived, although neither the energy, nor the lifetime of the triplet states of the donor molecules has been measured. It is, of course, possible that the energy of this resulting state is given up through non-radiative means. The validity of a steady state assumption under these conditions would have to be carefully considered. The exponential decay of the quenched triplet coupled with the presumed low probability of energy transfer and the ability to assume a steady state population of donor molecules are potentially good evidence to support charge transfer with immediate geminate recombination as the quenching process.

The quantum efficiencies calculated are still meaningful, it merely requires that the original assumptions that they were based upon are modified and that the terms are carefully defined. Optical limiting by RSA requires that a transient species be created that can bring about non-linear absorption of the system. These transients have been thought of as the solvated charged states formed through photo induced charge transfer, therefore the quantum yield values generated by the isobestic point method, and to some degree, by comparing absorption maxima do indeed measure the necessary quantities. It is also possible to get an idea of how efficient the process could be if other pathways were not available to drain population. It may even be realistic to utilize the transients created,

such as the contact ion pairs, for limiting applications. Faster spectroscopy is clearly needed in order to study such systems in more detail.

CHAPTER 5

CONCLUSION

The goal of the project of which this thesis research is a part is to develop optical limiting devices through reverse satuarable absorption. Photo induced charge transfer between acceptor and donor molecules is currently a very promising avenue toward a practical device based on this methodology. In order to achieve this goal and to make intelligent decisions about the synthesis of molecules and the advancement of materials, a good understanding of the physical processes that govern the behavior of the molecular systems is necessary.

Initial assumptions were made regarding the polarizability of molecules, their stability as ions, the conjugation of the molecule as a whole and of its components and the relationship of these parameters to the electron transfer rate and quantum efficiency of the system. These qualities, including the ground and excited state transmission and the molecule's durability are equally important to the success of a molecule as an optical limiter. Thus, it was the charge of this research group to test these assumptions about the structure-function relationship and to refine them as needed.

Basic measurements are first required, including the ground state transmission as well as the position of the excited state absorption and the degree of overlap between the two. Through absorption measurements, doping studies and photo induced absorption

experiments the ground state absorption was determined to be at an acceptable transmission level and the polaron absorption was close enough in frequency to the absorption of the neutral of C_{60}.

Kinetic analysis of the processes has allowed for some interesting conclusions to be drawn. The quenching of the C_{60} triplet state for all of the systems is diffusion limited and increases with an increase in molecular size and the number of chromophores on each molecule. There does not appear to be a direct correlation between the number of chromophores on the molecule and the rate at which the reaction occurs though. It is not possible to draw a conclusion regarding a ratio between the size of the molecule and the rate constant as the radius is not known. For now, it is best to stick to general trends. This process was originally referred to as merely "forward electron transfer", however it actually includes the processes of diffusion, actual transfer of the charge, solvation and any other quenching mechanisms. The rate constant for reverse electron transfer by ion recombination, which includes diffusion and the actual transfer of the charge, is also diffusion limited and roughly decreases with the size and the number of chromophores per molecule. Again, direct correlations cannot be drawn, as is the case with forward electron transfer. The analysis of this process yielded very interesting behavior associated with the Kn2 dendrimer and the Kn3 dendron and dendrimer. These molecules deviate from the expected kinetic model of a second order recombination of an anion and a cation. A couple of hypotheses have been postulated to explain this behavior. The first is a reaction between the radical cations to form a new molecule. This rate constant should be smaller than the diffusion limited forward and backward electron transfer rate

constants that involve neutral and oppositely charged molecules, respectively. This fact is possibly supported by the data, depending on how it is analyzed. In addition, such a mechanism could be confirmed by fitting the decay of the anion peak and the presence of a final product if it is stable enough to characterize. The second theory is that the dendron and dendrimer are supporting more than one charge per molecule. It has been shown that the chromophore "arms" act independently in absorption and doping studies [10], therefore it is possible that they could each carry a charge and behave much like a polaron even though technically part of the same molecule. Of course, two charges in such close proximity is coulombically unfavorable which may be why the deviation from the proposed kinetics is only seen in the more conjugated, larger chromophores. Again, more careful fitting of the anion and cation peaks with this hypothesis in mind could lead to confirmation of this mechanism.

The quantum yield calculations gave interesting results and led to the refinement of mechanisms and definitions. The quantum yield calculated using the quenching rates of the C_{60} triplet in solution with a donor molecule compared to C_{60} in solution alone indicated an efficiency from ~15% - ~70% depending on the compound. The efficiency also seemed to increase from oligimer to dendrimer and with an increase in concentration.

The quantum efficiency of the system was significantly lower when the maximum absorption of the solvated ions was compared to the number of C_{60} triplet molecules excited. Also, there was no clear dependence of efficiency on the type of molecule,

although, this method was prone to more error due to the very low concentration and therefore absorption signal of the solvated cations.

Similarly, the isobestic point method also gave lower quantum efficiency values for the Kn3 molecules. They are slightly higher than those numbers given by $[D^+]_{max}/[A^*]_{max}$ because back electron transfer through recombination had not become a significant factor in the absorption magnitude. The discrepancy between the latter two quantum efficiency calculations and the first method still exists. It was concluded that this is true because they are in essence measuring different things: the first measures triplet quenching while the latter measures ions solvated. It was originally assumed that the processes that quench the triplet ultimately gives solvated ions. Clearly, this is not the case, and by contrast only a few percent do. Therefore, other quenching processes have been proposed including electron transfer without solvation and energy transfer. Electron transfer very often yields a contact ion pair that can be either in direct contact, a contact radical ion pair (CRIP) or separated by a single solvent layer, a solvent separated radical ion pair (SSRIP) [22-25]. These can then undergo geminate recombination where the electron is transferred back before solvation into the bulk can take place. In this instance, ions are produced, but our current method of PIA analysis can not detect them. Energy transfer between a triplet molecule and a neutral would also lead to quenching without solvated ion formation and may or may not be detectable through emission. Nonetheless, it is clear that there are other processes besides electron transfer followed by solvation that must be considered when developing a cohesive and comprehensive mechanism for electron transfer in these organic systems.

REFERENCES

1. N.S. Sariciftci and A.J.Heeger, in *Handbook of Organic Conductive Molecules and Polymers Vol. 1: Charge-Transfer Salts, Fullerenes and Photoconductors.*, ed. H.S. Nalwa, John Wiley and Sons, 1997, pp. 413-457.

2. J. R. Bolton and M. D. Archer, in *Electron Transfer in Inorganic, Organic and Biological Systems.,* ed. J.R.Bolton, N.Mataga, G.McLendon, American Chemical Society, 1991, pp. 7-24.

3. R.A.Marcus, *J.Chem.Phys.*, 1956, **24**, 966.

4. N.S.Hush, *Trans.Faraday.Soc.*, 1961, **57**, 557.

5. L. Eberson, in *Advances in Physical Organic Chemistry. Vol. 18.*, ed. V.Gold and D. Bethell, Academic Press, 1982, pp.79-185.

6. *Chemical Kinetics and Dynamics, Second edition.*, ed. J.I. Stienfeld, J.S.Francisco, W.L.Hase. Prentice Hall, 1999, pp.124-143.

7. N.S.Sariciftci, L.Smilowitz, A.J.Heeger, F.Wuld, *Science*, 1992, **258**, 1474.

8. M.Fujitsuka, C. Luo, O.Ito, *J.Phys.Chem. B*, 1999, **103**, 445.

9. W. Sonnenberg, Masters Thesis. Montana State University, 2000.

10. K.Ashworth, *Synthesis of Dendrons and Dendrimers Incorporating Diphenylamino-N-Ethyl –N- Hydroxyethylaminodiphenylpolyenes for Photonic Application.* Masters Thesis, Montana State University, 2000.

11. J.Bonvoisin, J.P.Launay, W. Verbouwe, M. Van der Aurweraer, F.C. de Schryver, *J.Phys.Chem.*, 1996, **100**, 17079.

12. J.Bonvoisin, J.P.Launay, M. Van der Aurweraer, F.C. de Schryver, *J.Phys.Chem.*, 1994, **98**, 5052.

13. N.S.Hush, *Chemical Physics*, 1975, **10**, 361.

14. N.S. Hush, *Prog. Inorg. Chem.* 1967, **8**, 391.

15. R.A.J.Janssen, D. Moses, N.S.Sariciftci, *J.Chem.Phys.*, 1994, **101**, 9519

16. M. El-Kemary, M Fujitstuka, O.Ito, *J.Phys.Chem.* 1999, **103**, 1329.

17. O.Ito, Y. Sasahi, Y. Yoshikawa, A Watanabe, *J.Phys.Chem.*, 1995, **99**, 9838.

18. V.Wintgens, P.Valat, F.Garnier, *J.Phys.Chem.*, 1994, **98**, 228.

19. T. Ebbesen, K.Tanigaki, S.Kuroshima, *Chem.Phys.Let.* 1991, **181**, 501.

20. M.Fujitsuka, C.Luo, O.Ito, Y.Murata, K.Kamatsu, *J.Phys.Chem.*, 1999, **103**, 7155.

21. L.Spangler, Y.Han, *J.Phys.Chem.A.*, submitted for publication.

22. I.R.Gould and S.Farid, *Acc.Chem.Res.*, 1996, **29**, 522.

23. J.Mattay, M.Vondenhof, in *Photoinduced Electron Transfer III*, ed. J.Mattay,

24. Springer-Verlag, 1990, pp-218-252.

25. I.Gould, R.H.Young, R.E.Moody, S.Farid, *J.Phys.Chem.*, 1991, **95**, 2068.

26. I.Gould, R.H.Young, L.J.Mueller, S.Farid, *J.Am. Chem.Soc.*, 1994, **116**, 8176.

27. H.Masuhara, N.Mataga, *Acc.Chem Res.*, 1981, **14**, 312.

MONTANA STATE UNIVERSITY - BOZEMAN
3 1762 10337696 6